Supporting Information

Chiral blue box host-guest encapsulation induced CPL from achiral planar fluorescence dyes

Qing Yang,[a] Jingya Li,[b] Yanni He,[c] Ting Gao,[a] Yanyan Zhou*[a] and Hongfeng Li*[a]

a Key Laboratory of Functional Inorganic Material Chemistry, Ministry of Education, Heilongjiang University, 74, Xuefu Road, Harbin 150080.
b China State Key Laboratory of Baiyunobo Rare Earth Resource Researches and Comprehensive Utilization Institution, Baotou, 014030, China.
c Hwa Chong International School, 269783 Singapore.
E-mail: lihongfeng1@hlju.edu.cn; zhouyanyan@hlju.edu.cn; gaotingmail@sina.cn; jingya1100@163.com

Table of contents

1. Experimental section

1.1 Methods

^{1}H NMR and ESI-TOF-MS

The ^{1}H NMR spectra were recorded on a Bruker AVANCE III 400 MHz spectrometer. ^{1}H NMR chemical shifts are in ppm relative to tetramethylsilane (TMS): $CDCl_3$ (7.26 ppm for ^{1}H).

High-resolution electrospray ionization mass spectrometry (ESI-TOF-MS) were recorded by using a Bruker maXis mass spectrometer. Data analysis was conducted with the Mass-Lynx Data Analysis software (Version 4.1) and simulations were performed with the MassLynx Isotope Pattern software.

Optical Measurements

UV−Vis spectra were recorded at room temperature in different concentrations of CH_3OH solutions in 10 mm light path quartz cuvettes on a PerkinElmer Lambda 25 spectrometer.

Excitation and emission spectra were recorded using an Edinburgh FLS 980 fluorescence spectrometer equipped with a red-sensitive photomultiplier detector (Hamamatsu R928). Excitation spectra were measured in CH_3OH solutions (c = 2.5 × 10^{-5} M) with quartz cuvettes of 10 mm path length. Emission spectra were measured in different concentrations of CH_3OH solutions with quartz cuvettes of 10 mm path length.

Luminescence lifetimes were recorded on a single photon counting spectrometer from Edinburgh Instruments (FLS 980) with a microsecond pulse lamp as the excitation source.

Chiraloptical measurements

CD and CPL experiments were performed on an Olis DM245 spectrometer at room temperature. All samples were dissolved in different concentrations of Methanol or CH_3CN solutions, and quartz cuvettes with optical pathway of 10 mm were employed. CD spectra were recorded in the range of 280−450 nm and in increments of 1 nm, and a slit width of 2 mm for the excitation was utilized. CPL spectra were recorded with a 375 nm laser as light source. The emission of left- and right-handed polarized light were collected in the range of 400−700 nm with the integration time of 1 s and the emission slit width of 0.6 mm.

1.2 The synthetic routes of binaphthol unit and the characterization of corresponding intermediates.

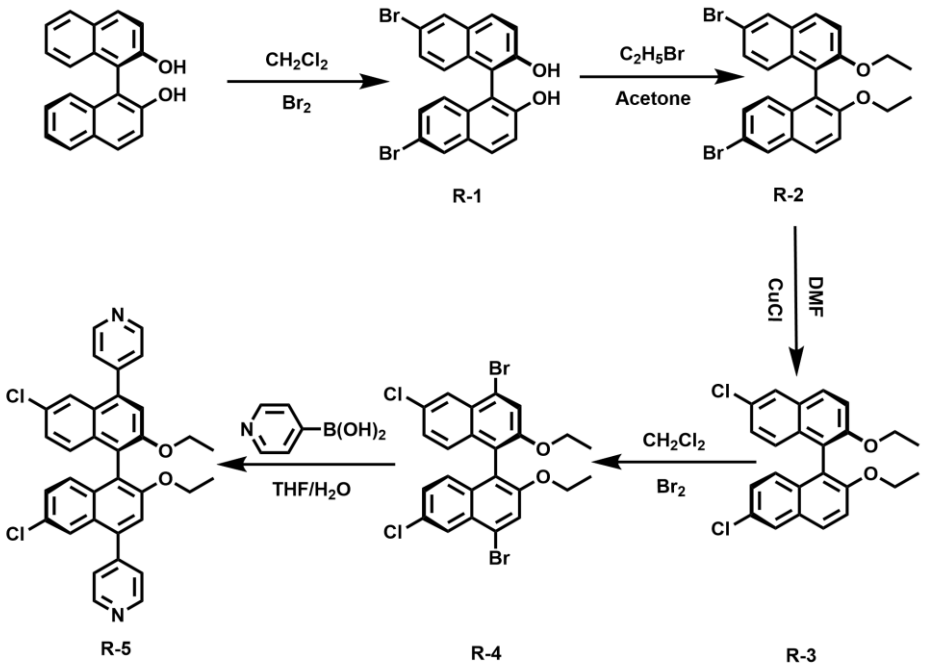

Scheme S1. Synthetic route of R-5.

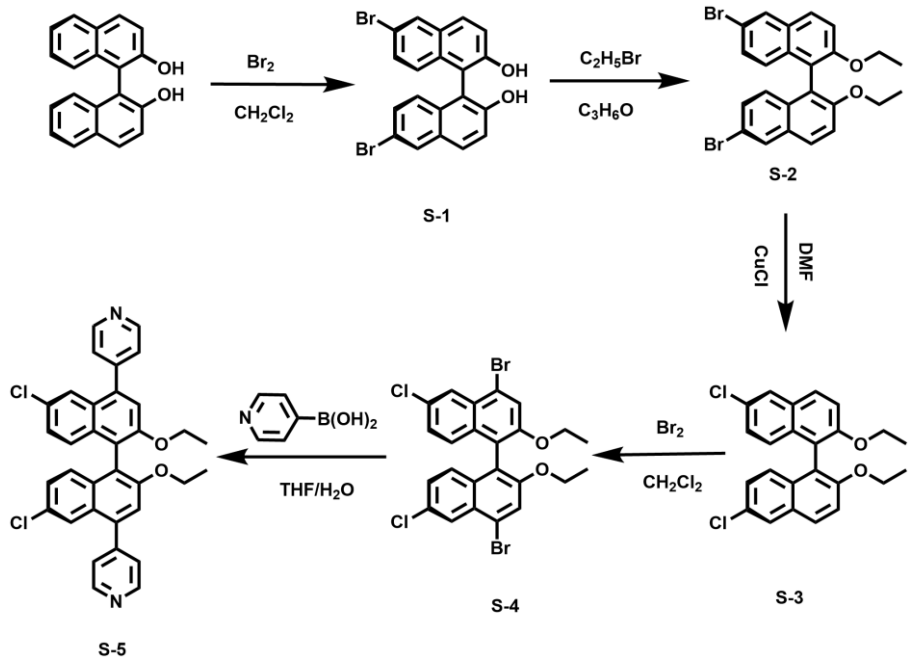

Scheme S2. Synthetic route of S-5.

1.2.2 Characterization of the corresponding intermediates.

1.2.2.1 (R)-6,6'-Dibromo-1,1'-binaphthalene-2,2'-diol (R-1)

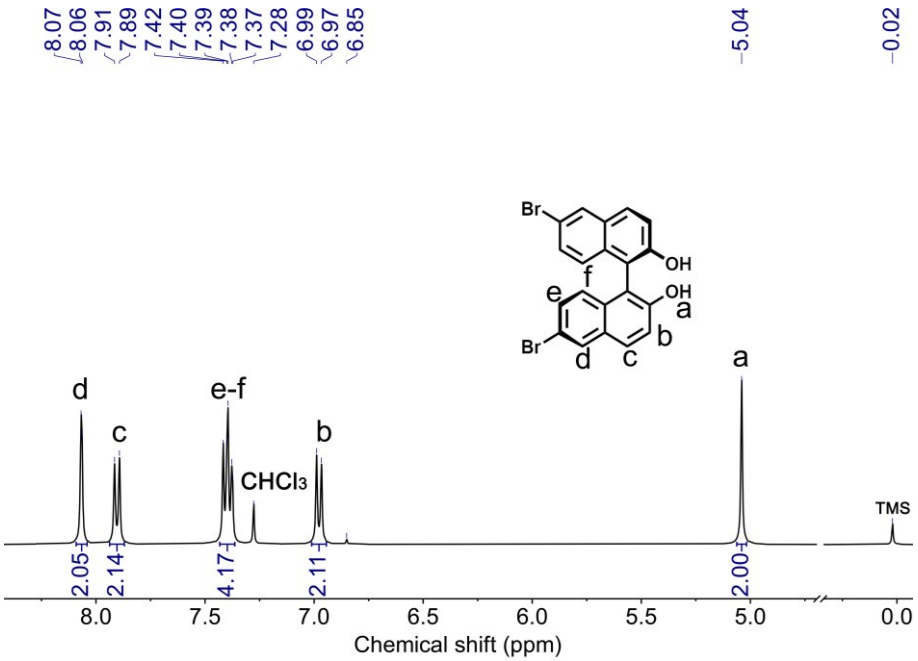

Fig. S1. ^{1}H NMR spectrum (400 MHz, 298 K, $CDCl_3$) of R-**1**.

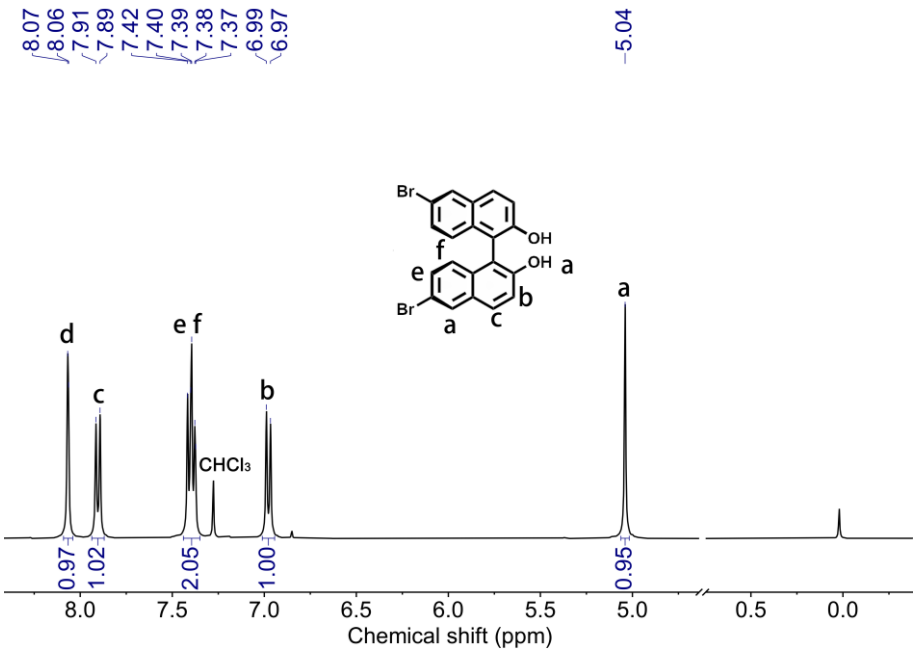

Fig. S2. ^{1}H NMR spectrum (400 MHz, 298 K, $CDCl_3$) of S-**1**.

1.2.2.2 (R)-6,6'-dibromo-2,2'-diethoxy-1,1'-binaphthalene (R-2)

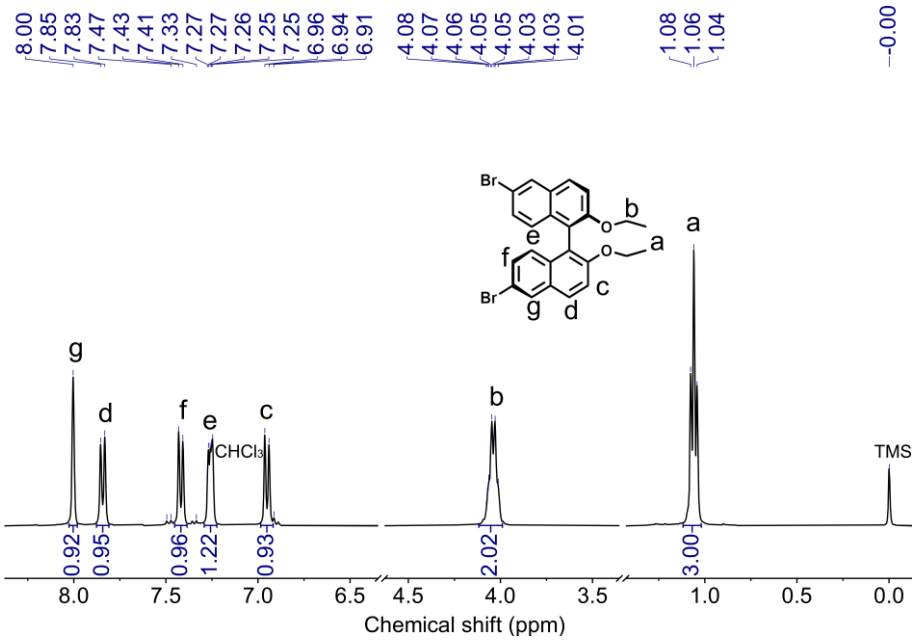

Fig. S3. ^{1}H NMR spectrum (400 MHz, 298 K, $CDCl_3$) of R-**2**.

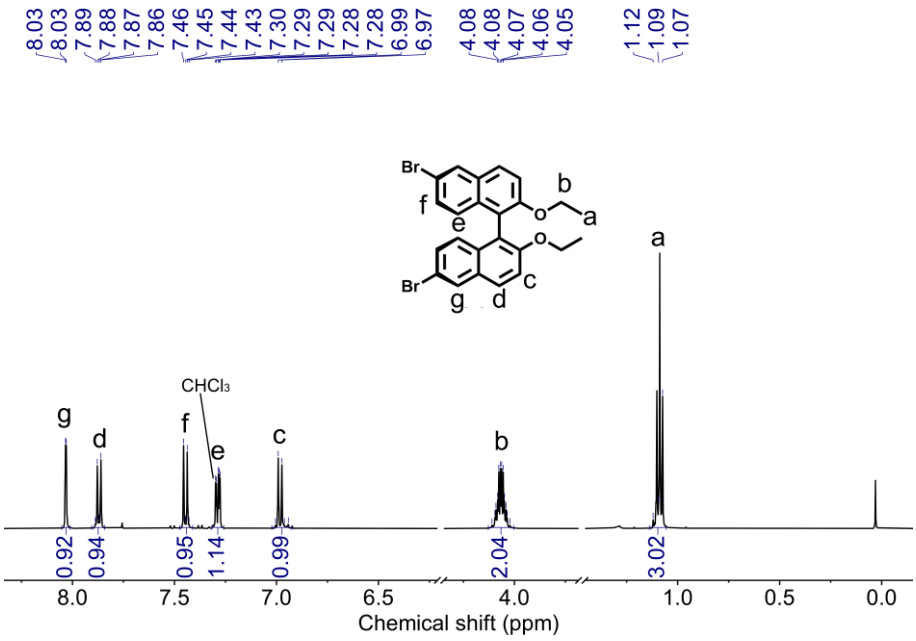

Fig. S4. ^{1}H NMR spectrum (400 MHz, 298 K, $CDCl_3$) of S-**2**.

1.2.1.3 (R)-6,6'-dichloro-2,2'-diethoxy-1,1'-binaphthalene (R-3)

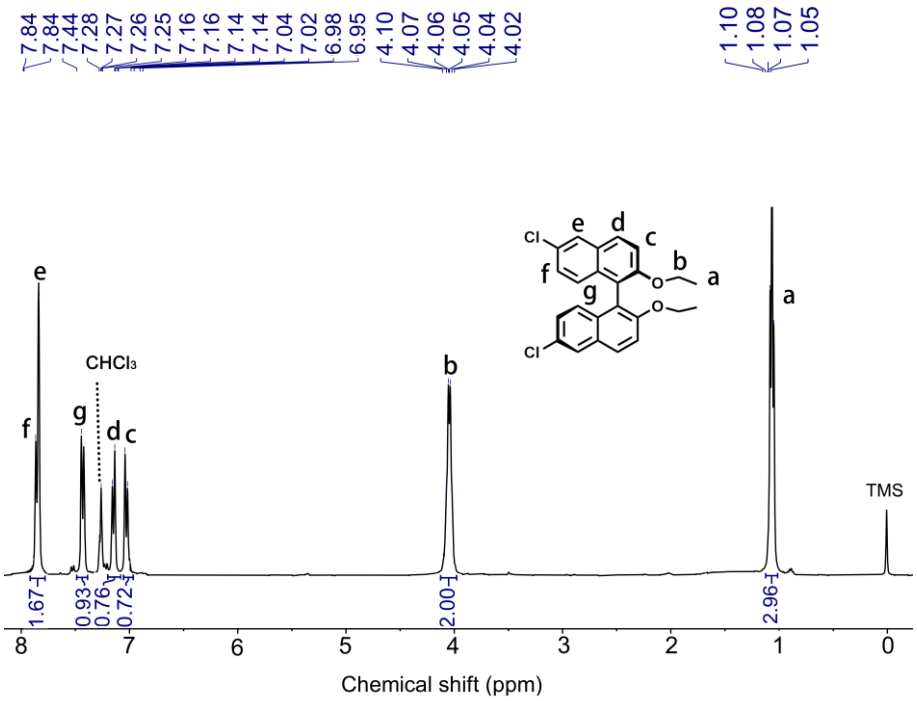

Fig. S5. ^{1}H NMR spectrum (400 MHz, 298 K, $CDCl_3$) of R-**3**.

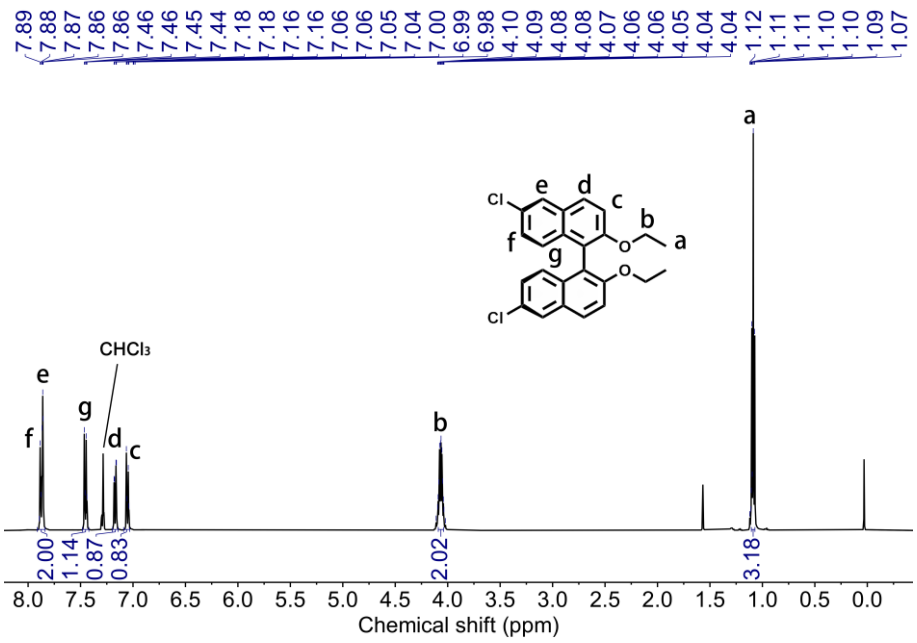

Fig. S6. ^{1}H NMR spectrum (400 MHz, 298 K, $CDCl_3$) of S-**3**.

1.2.2.4 (R)-4,4'-dibromo-6,6'-dichloro-2,2'-diethoxy-1,1'- binaphthalene (R-4)

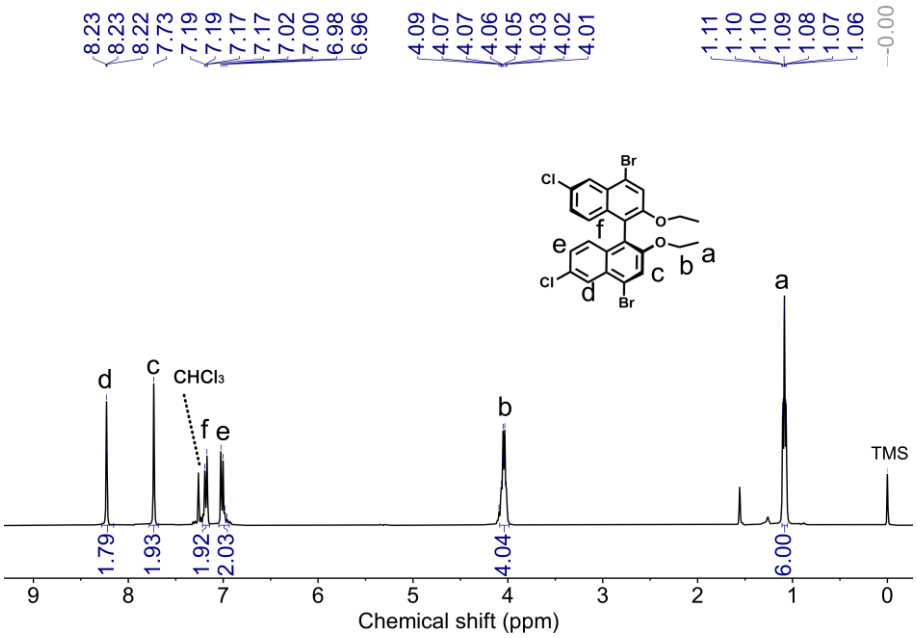

Fig. S7. ^{1}H NMR spectrum (400 MHz, 298 K, $CDCl_3$) of R-**4**.

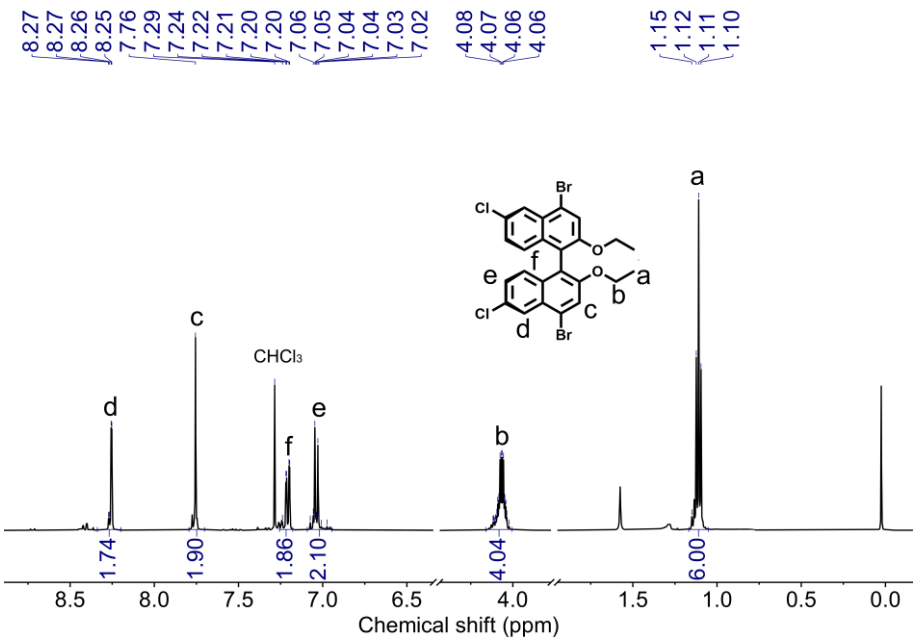

Fig. S8. ^{1}H NMR spectrum (400 MHz, 298 K, $CDCl_3$) of S-**4**.

1.2.2.5 (R-5)-4,4'-(6,6'-dichloro-2,2'-diethoxy-[1,1'-binaphthalene]-4,4'-diyl)dipyridine

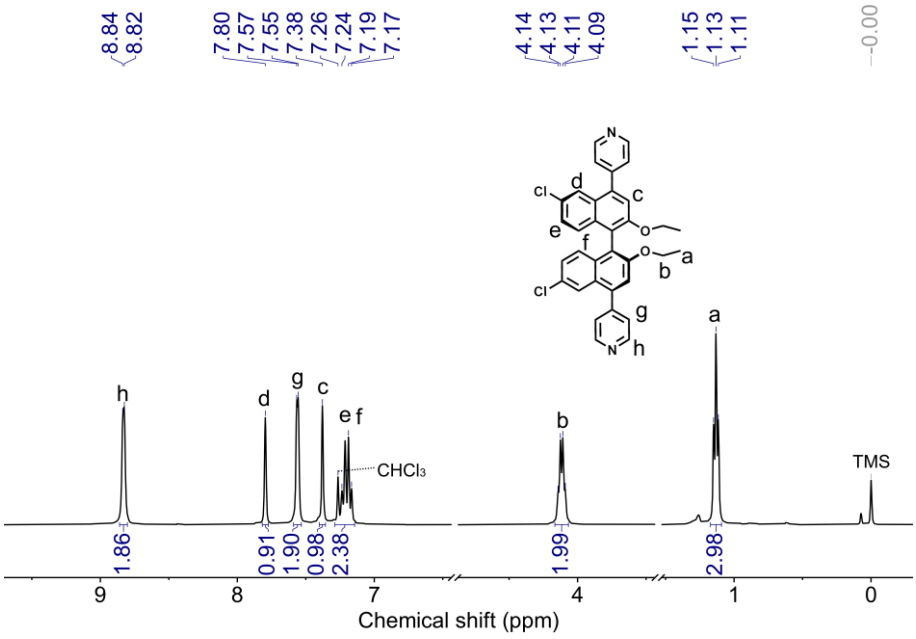

Fig. S9. ^{1}H NMR spectrum (400 MHz, 298 K, $CDCl_3$) of R-**5**.

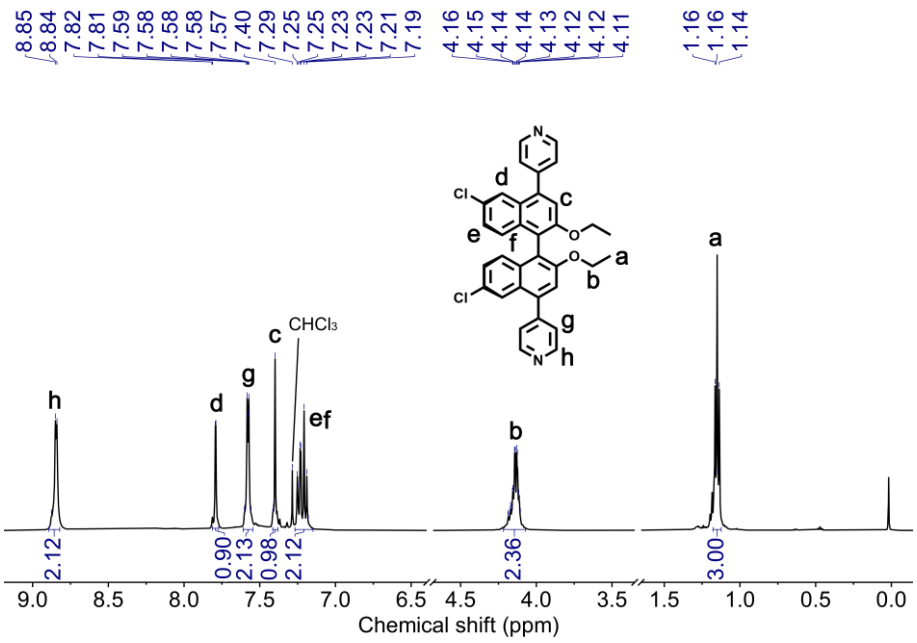

Fig. S10. ^{1}H NMR spectrum (400 MHz, 298 K, $CDCl_3$) of S-**5**.

1.3 The synthetic routes of chiral cyclophanes and the characterization of corresponding intermediates.

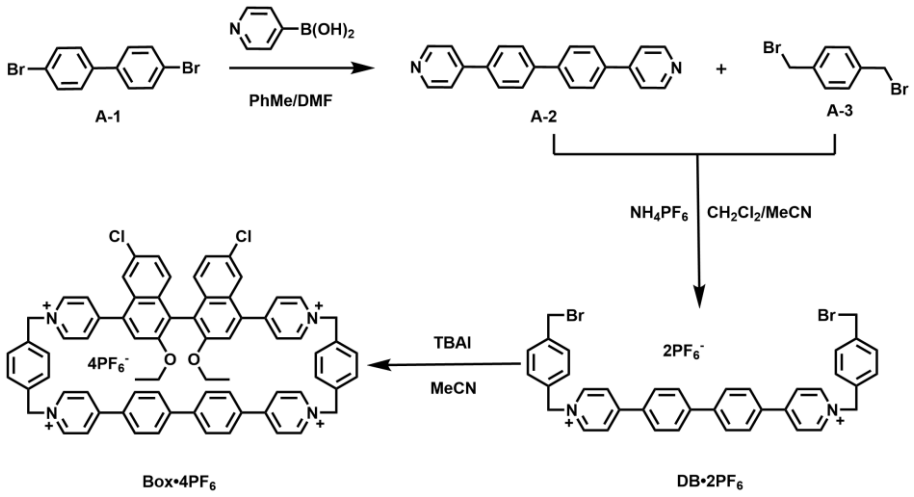

Scheme S3. Synthetic route of Binbox.

1.3.1 Characterization of the corresponding intermediates.

1.3.1.1 4,4′-(4,4′-Biphenylene)bipyridine (A-2)

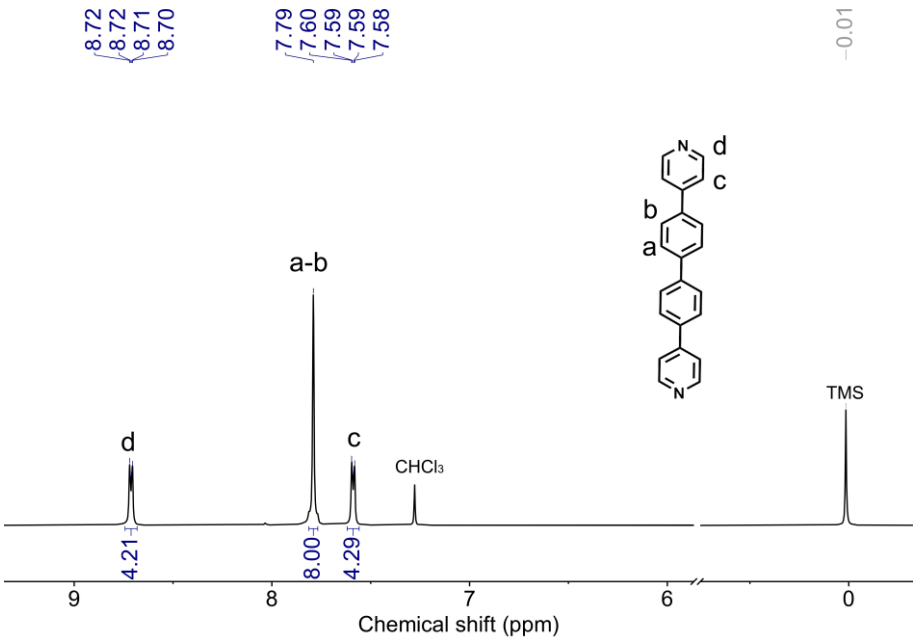

Fig. S11. ^{1}H NMR spectrum (400 MHz, 298 K, $CDCl_3$) of A-2.

1.3.1.2 Bis(4-bromomethylbenzyl)(4,4′-(4,4′-biphenylene)bipyridin-1-ium)bis(hexafluoro-phosphate) (DB•2 PF_6)

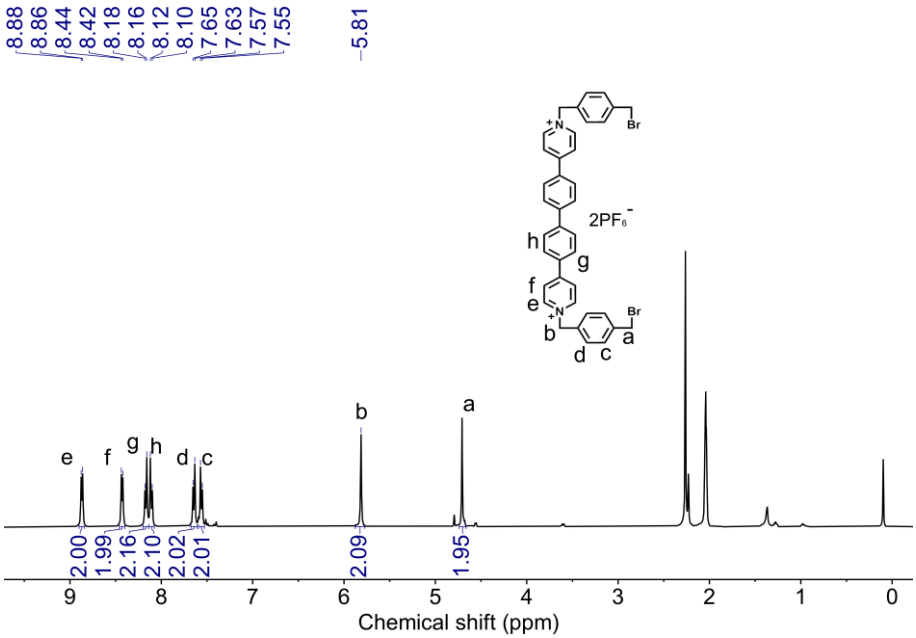

Fig. S12. ^{1}H NMR spectrum (400 MHz, 298 K, CD_3CN) of DB•2PF_6.

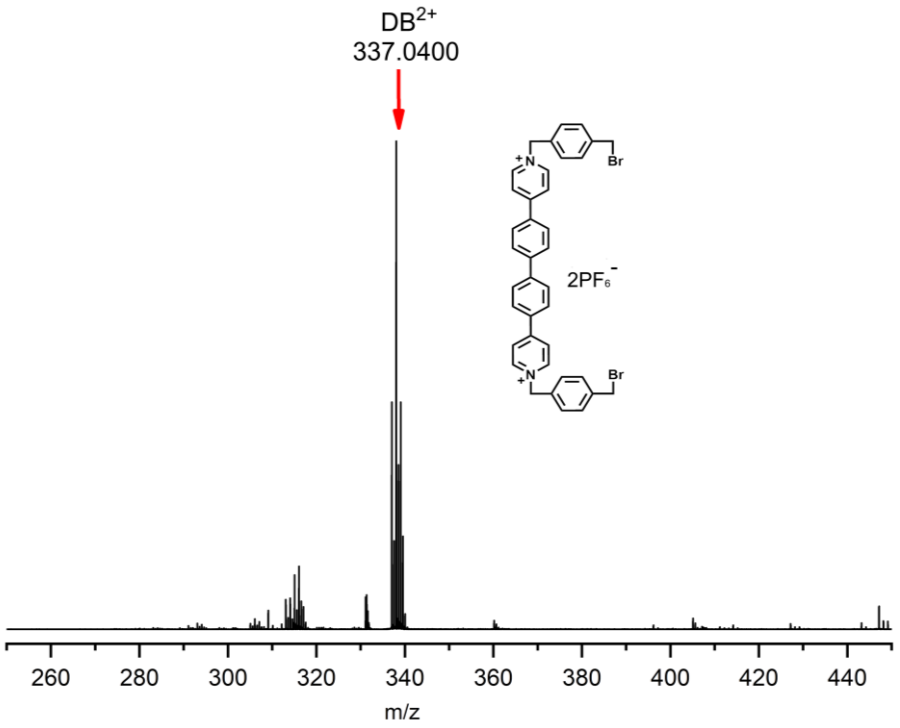

Fig. S13. ESI-TOF-MS spectrum of DB•2PF_6.

1.3.1.3 Binbox

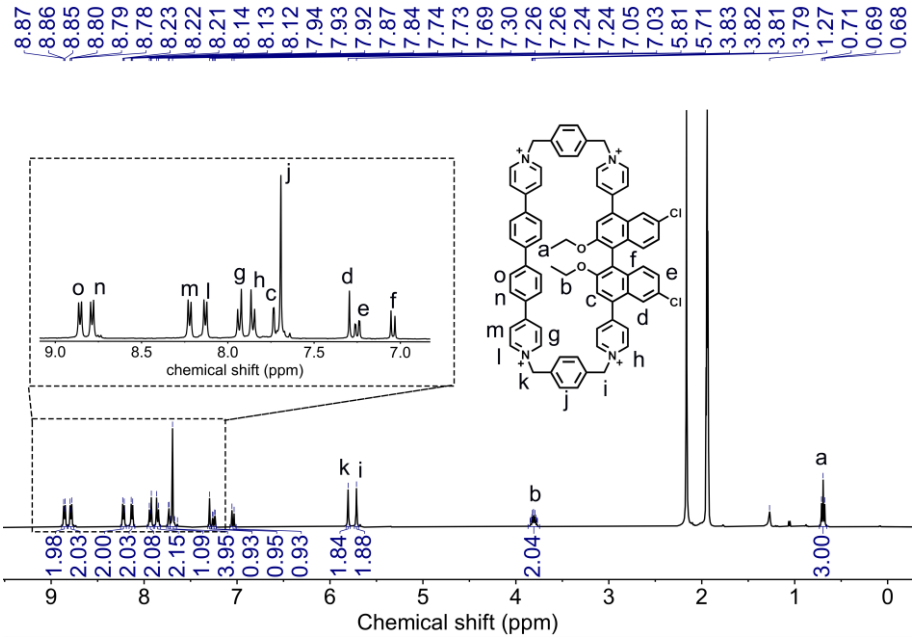

Fig. S14. ^{1}H NMR spectrum (400 MHz, 298 K, CD_3CN) of R-Binbox.

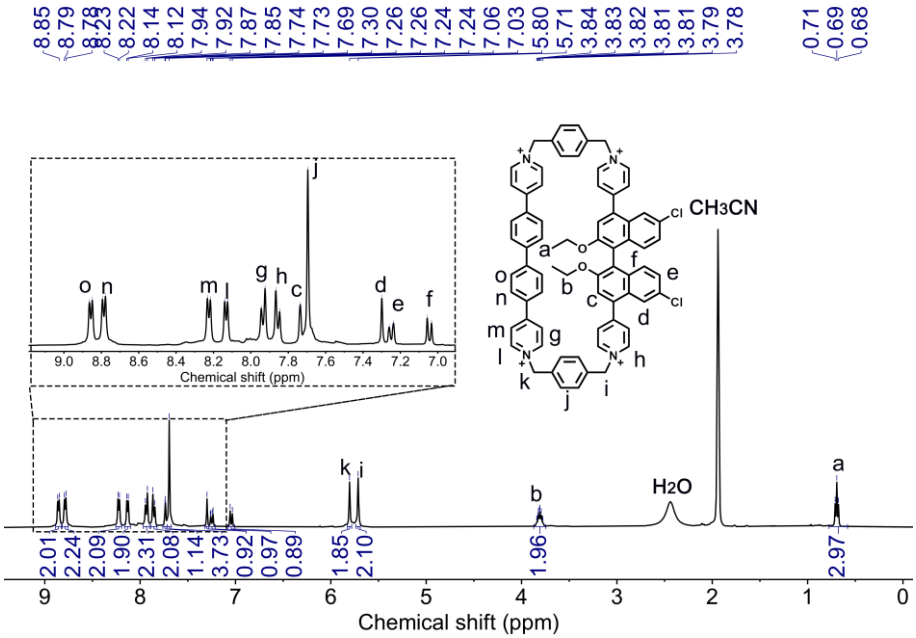

Fig. S15. ^{1}H NMR spectrum (400 MHz, 298 K, CD_3CN) of S-Binbox.

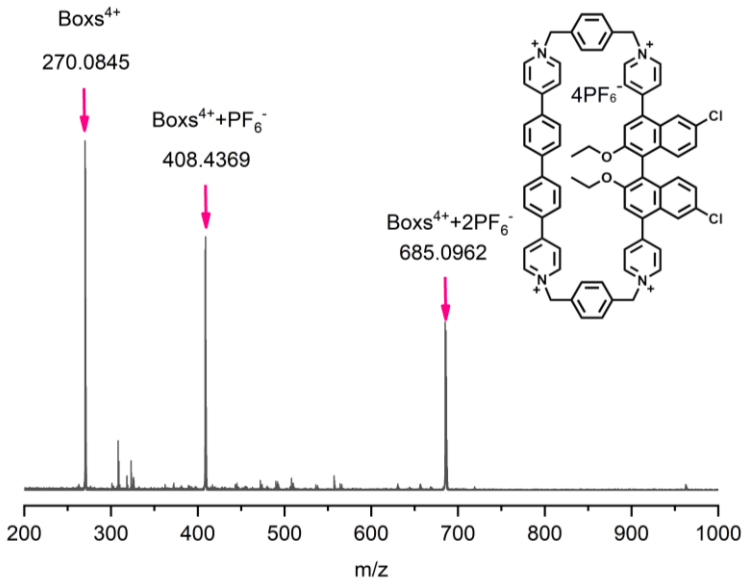

Fig. S16. ESI-TOF-MS spectrum of Binbox.

1.4 Synthesis and Characterization of achiral fluorescent dyes

1.4.1 Characterization of the corresponding intermediates

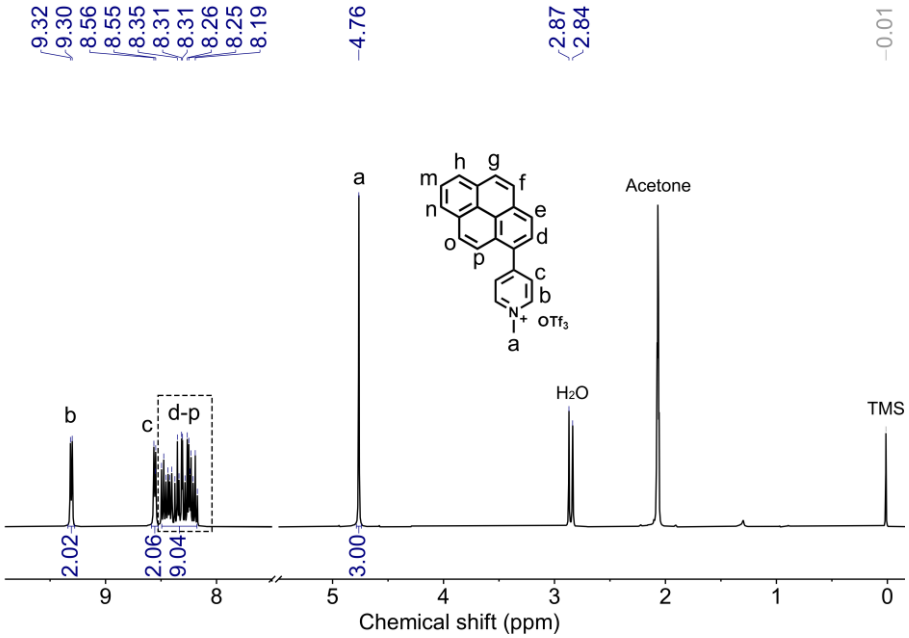

Fig. S17. ^{1}H NMR spectrum (400 MHz, 298 K, Acetone) of G1.

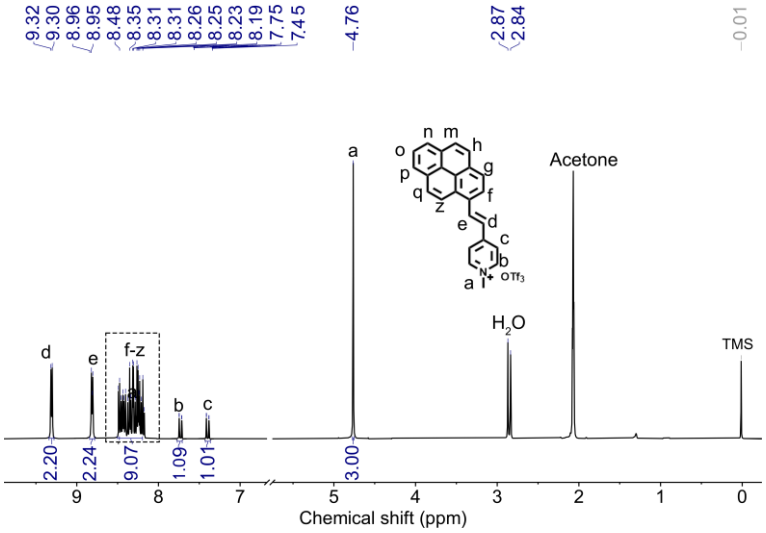

Fig. S18. [1]H NMR spectrum (400 MHz, 298 K, Acetone) of G2.

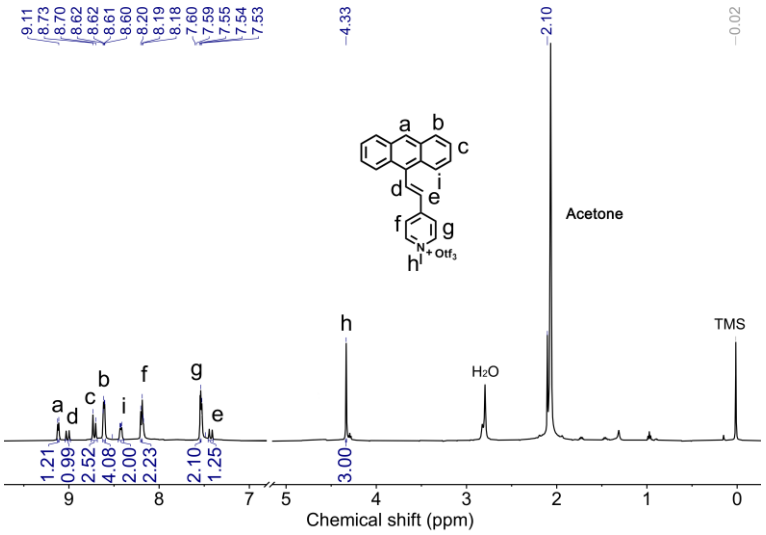

Fig. S19. [1]H NMR spectrum (400 MHz, 298 K, Acetone) of G3.

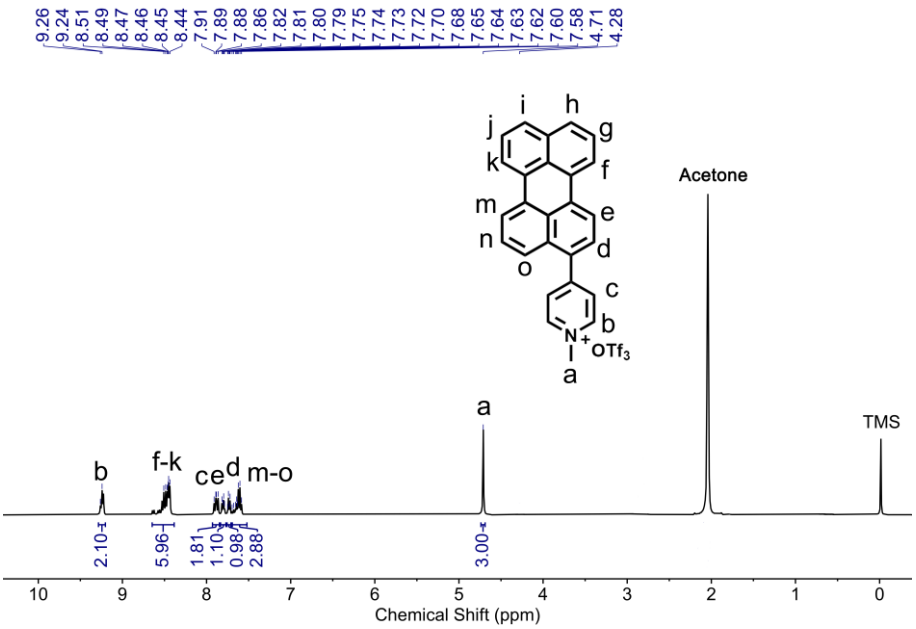

Fig. S20. [1]H NMR spectrum (400 MHz, 298 K, Acetone) of G4.

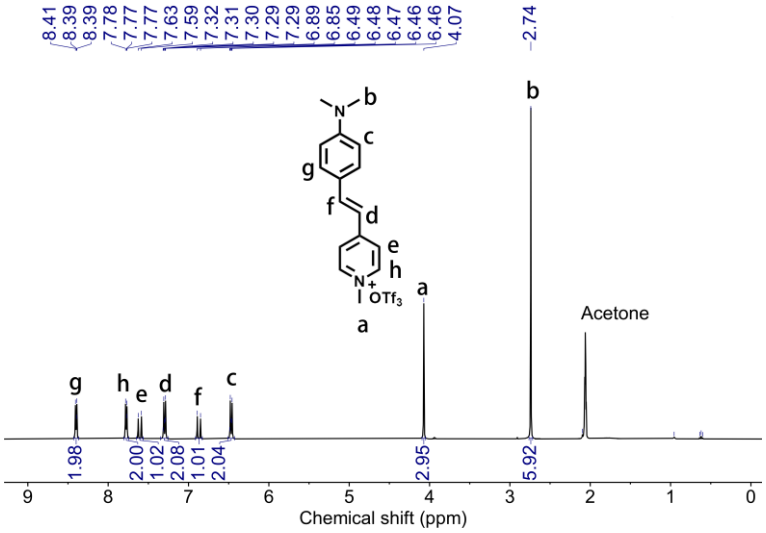

Fig. S21. ^{1}H NMR spectrum (400 MHz, 298 K, Acetone) of G5.

2. Photophysical properties of Binbox

2.1 UV-vis and CD spectra of host-guest combination

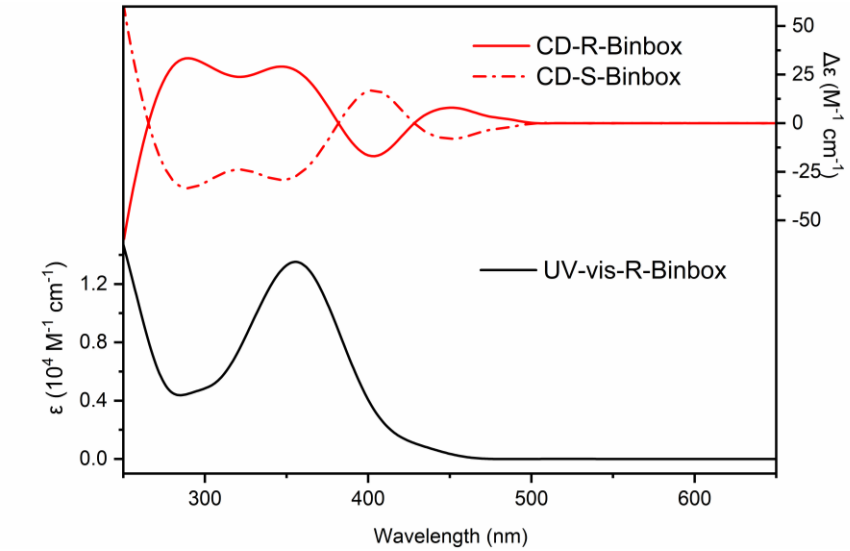

Fig. S22. UV-vis and CD spectra of the Binbox in CH_3OH ($c = 1.0 \times 10^{-5}$ M).

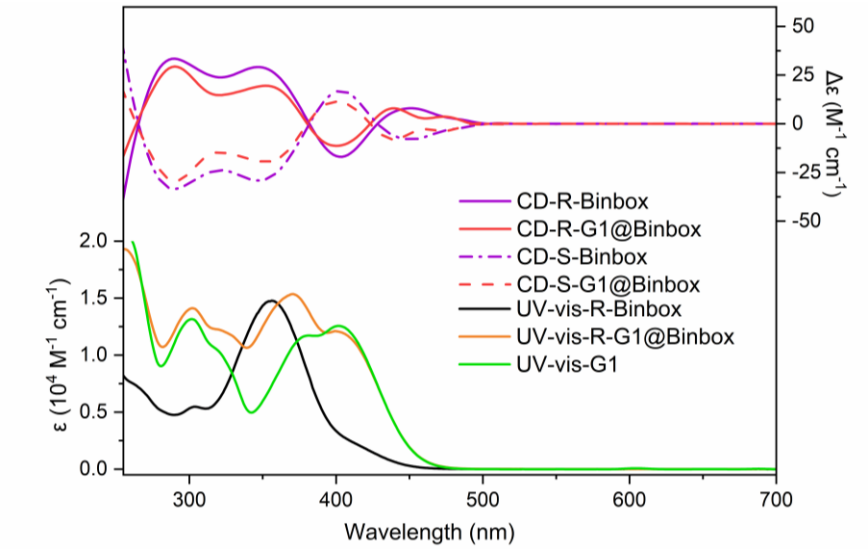

Fig. S23. UV-vis and CD spectra of the G1@Binbox in CH_3OH ($c = 1.0 \times 10^{-5}$ M).

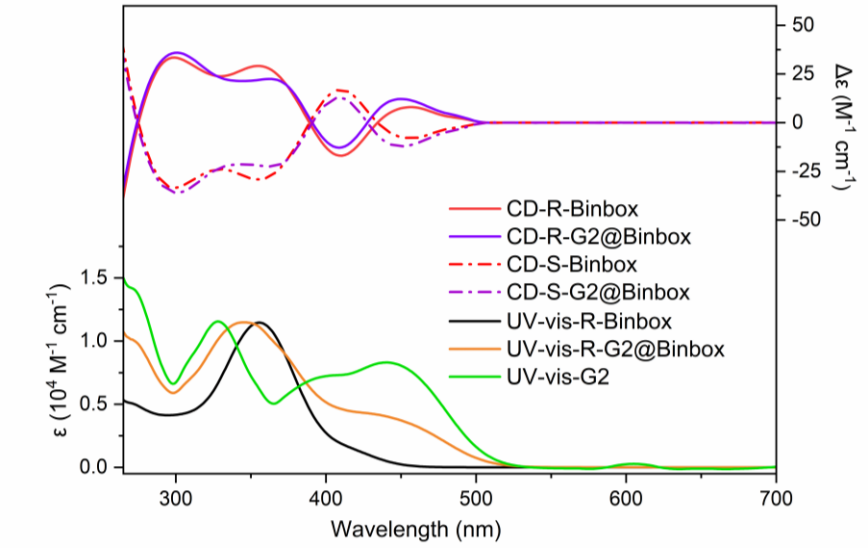

Fig. S24. UV-vis and CD spectra of the G2@Binbox in CH_3OH ($c = 1.0 \times 10^{-5}$ M).

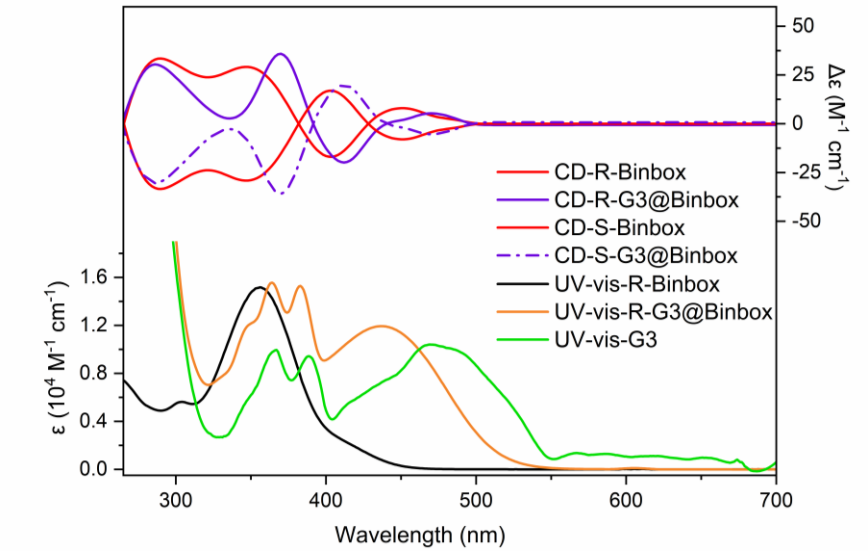

Fig. S25. UV-vis and CD spectra of the G3@Binbox in CH_3OH ($c = 1.0 \times 10^{-5}$ M).

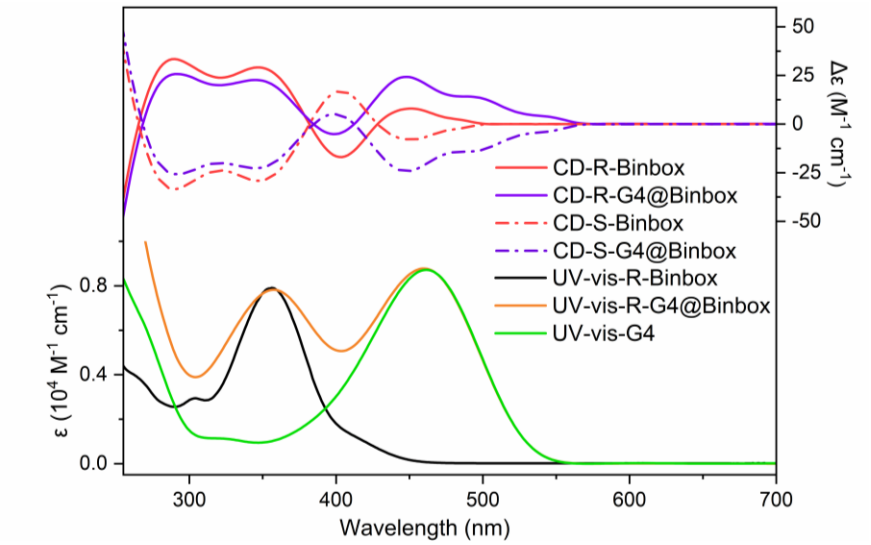

Fig. S26. UV-vis and CD spectra of the G4@Binbox in CH_3OH (c = 1.0 × 10^{-5} M).

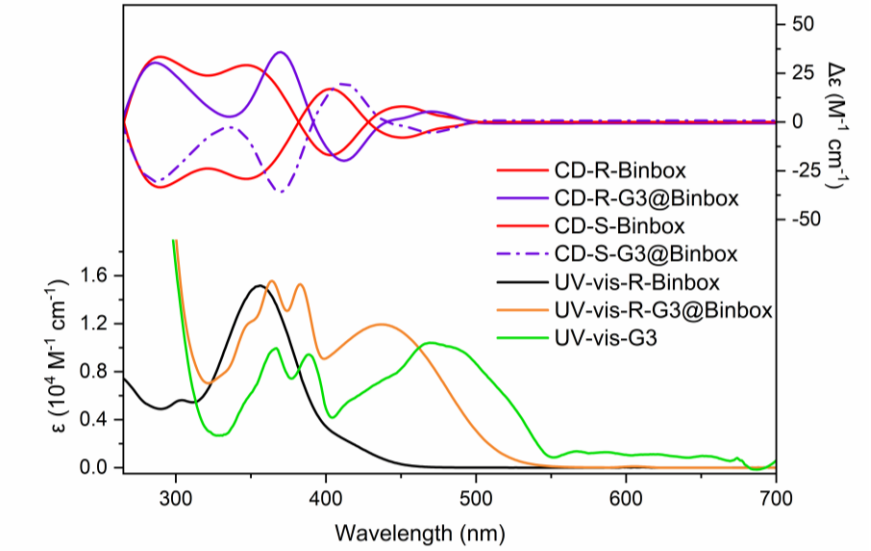

Fig. S27. UV-vis and CD spectra of the G5@Binbox in CH_3OH (c = 1.0 × 10^{-5} M).

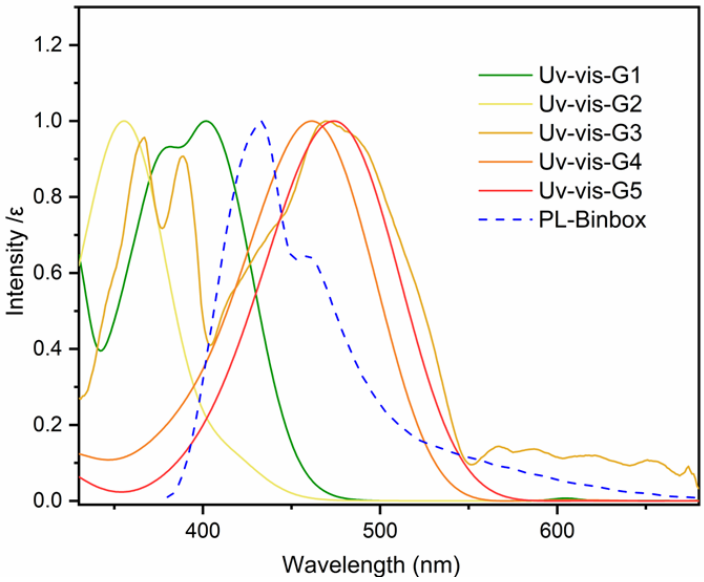

Fig. S28. UV-vis and CD spectra of the G1-G5 in CH_3OH (c = 1.0 × 10^{-5} M) and emission spectral of G1 to the

solution of Binbox in CH_3OH (c = 1.0 × 10^{-5} M).

2.2 Fluorescence spectra of host-guest combination

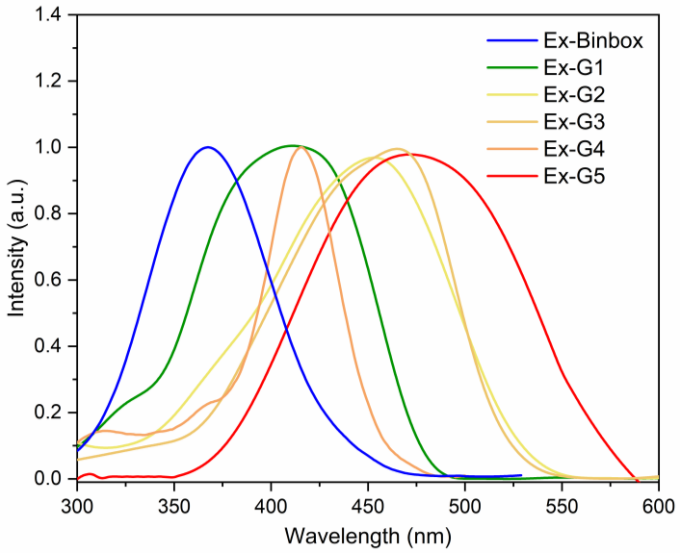

Fig. S29. Excitation and emission spectra of BInbox and G1-G5 in CH_3OH (c = 1.0 × 10^{-5} M).

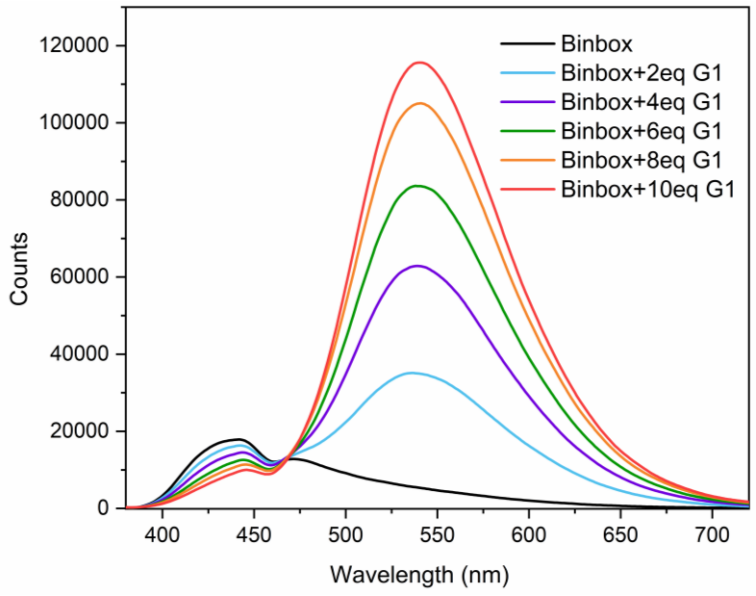

Fig. S30. Changes in emission spectral upon adding various equivalents of G1 to the solution of Binbox in CH_3OH (c = 1.0 × 10^{-5} M).

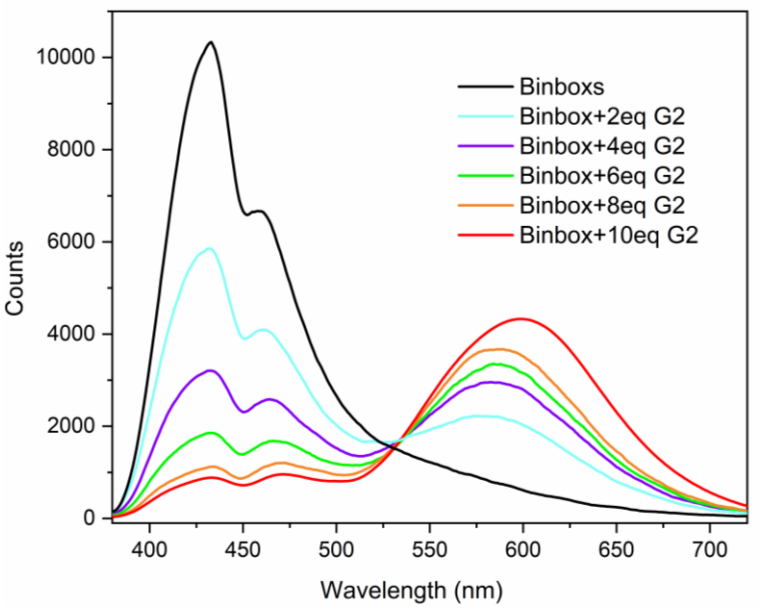

Fig. S31. Changes in emission spectral upon adding various equivalents of G2 to the solution of Binbox in CH_3OH ($c = 1.0 \times 10^{-5}$ M).

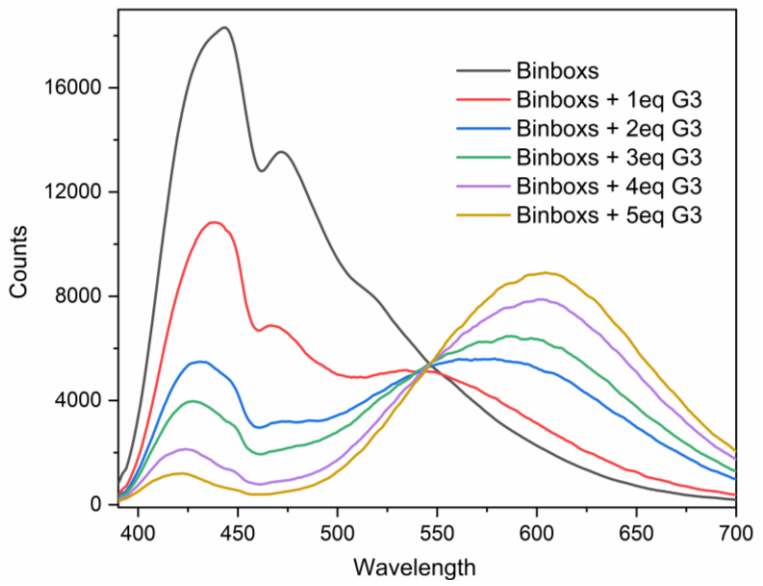

Fig. S32. Changes in emission spectral upon adding various equivalents of G3 to the solution of Binbox in CH_3OH ($c = 1.0 \times 10^{-5}$ M).

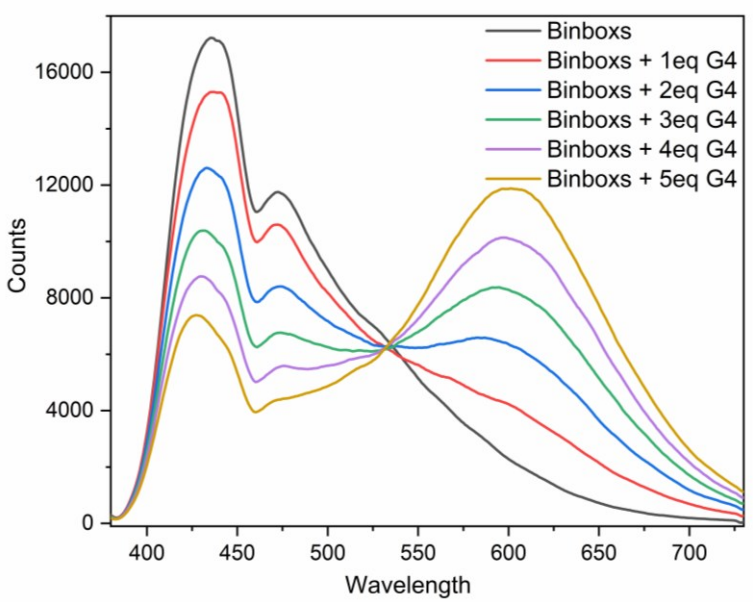

Fig. S33. Changes in emission spectral upon adding various equivalents of G1 to the solution of Binbox in CH_3OH ($c = 1.0 \times 10^{-5}$ M).

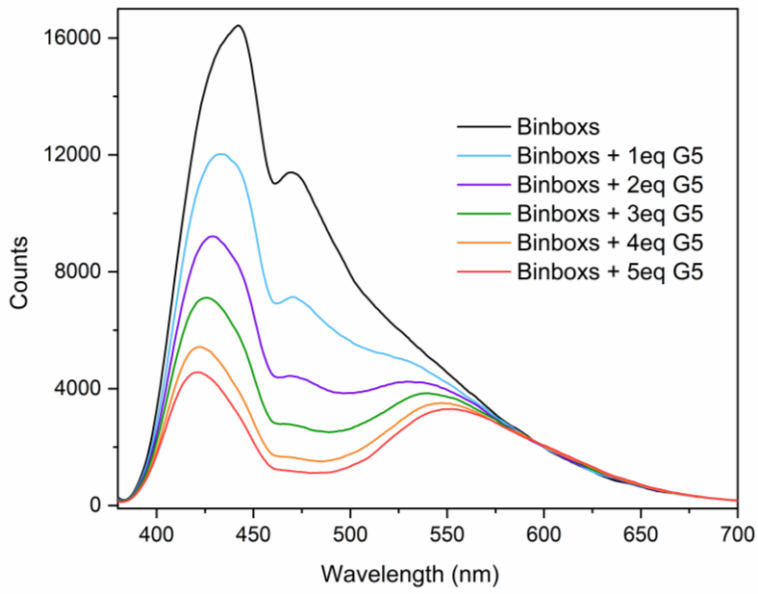

Fig. S34. Changes in emission spectral upon adding various equivalents of G1 to the solution of Binbox in CH_3OH ($c = 1.0 \times 10^{-5}$ M).

2.3 Time-correlated single photon counting decay profiles

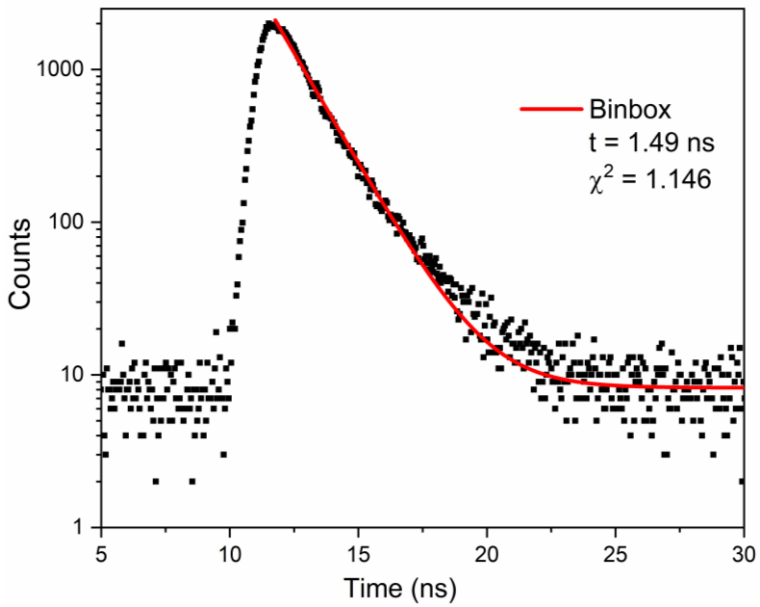

Fig. S35. Luminescence decay curves of Binbox in CH_3OH ($c = 1.0 \times 10^{-5}$ M).

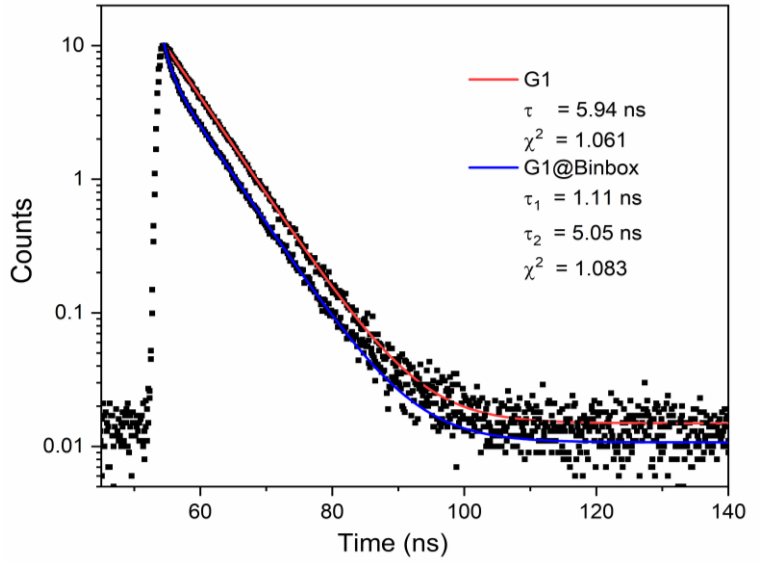

Fig. S36. Luminescence decay curves of G1@Binbox in CH_3OH ($c = 1.0 \times 10^{-5}$ M).

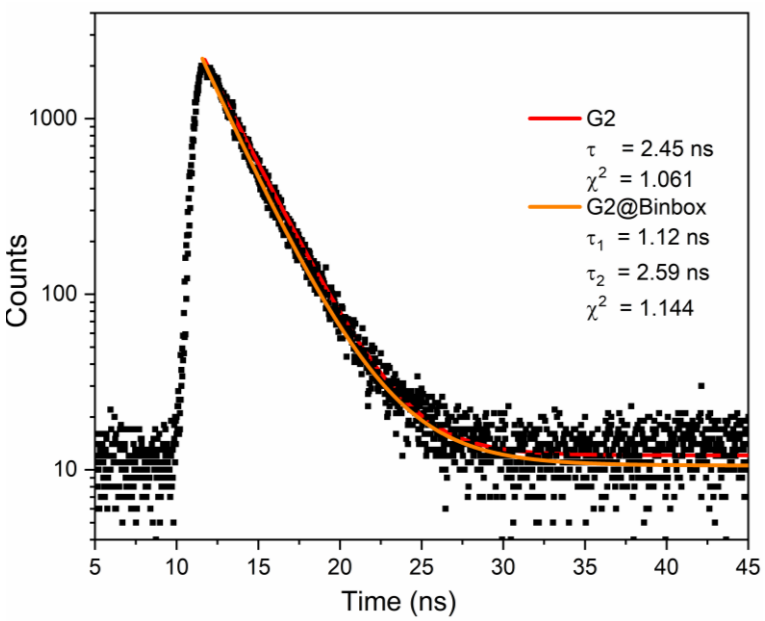

Fig. S37. Luminescence decay curves of G2@Binbox in CH_3OH (c = 1.0 × 10^{-5} M).

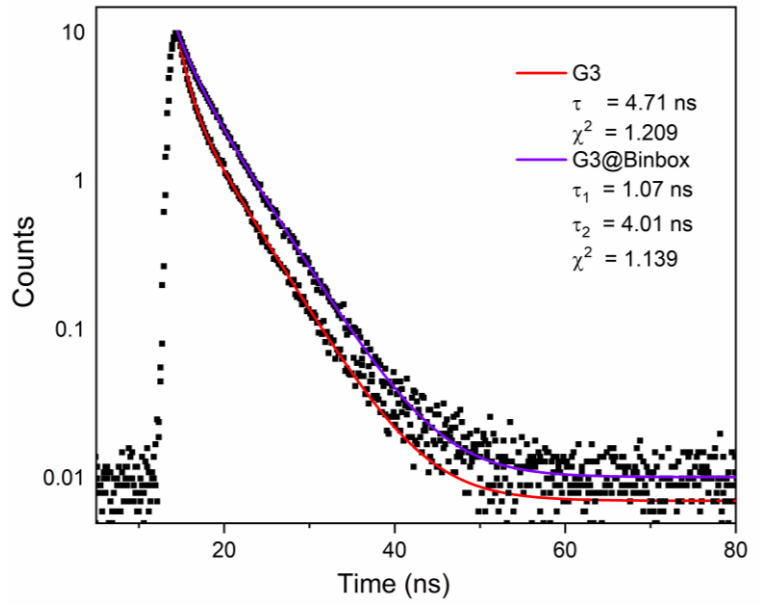

Fig. S38. Luminescence decay curves of G3@Binbox in CH_3OH (c = 1.0 × 10^{-5} M).

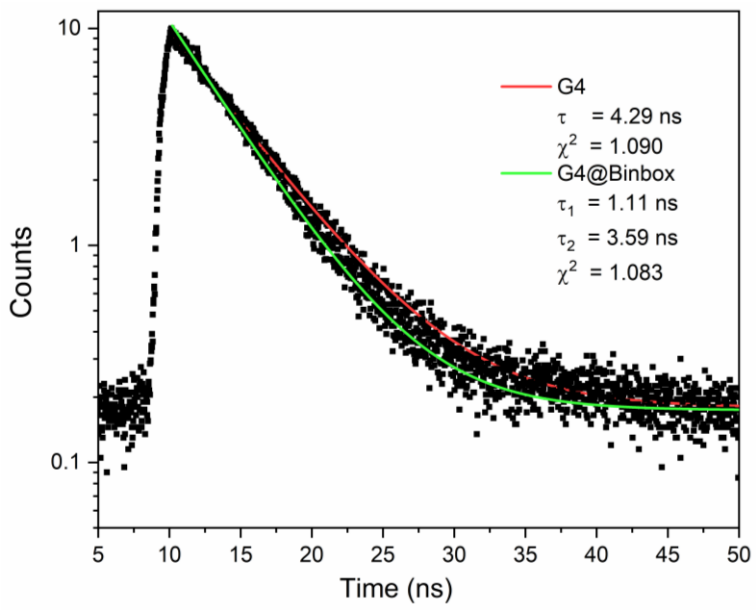

Fig. S39. Luminescence decay curves of G4@Binbox in CH_3OH (c = 1.0 × 10^{-5} M).

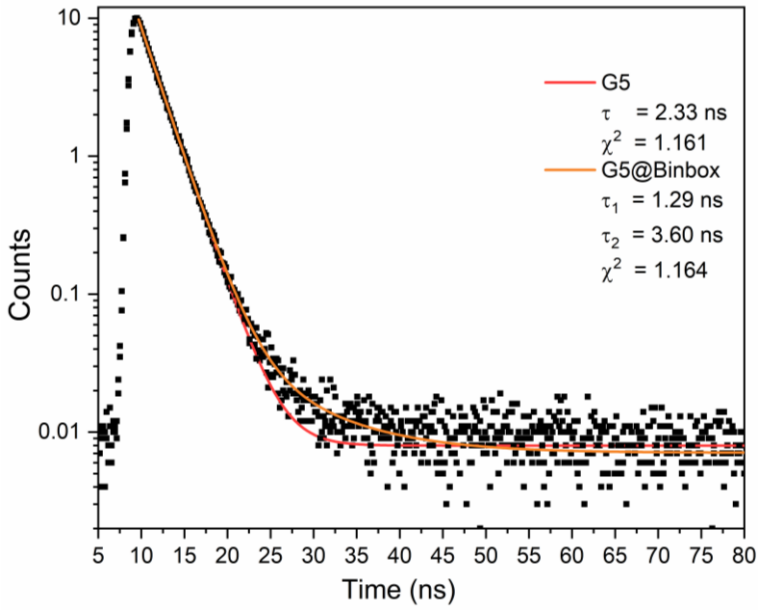

Fig. S40. Luminescence decay curves of G5@Binbox in CH_3OH (c = 1.0 × 10^{-5} M).

2.4 The screenshots of the luminescence quantum yield

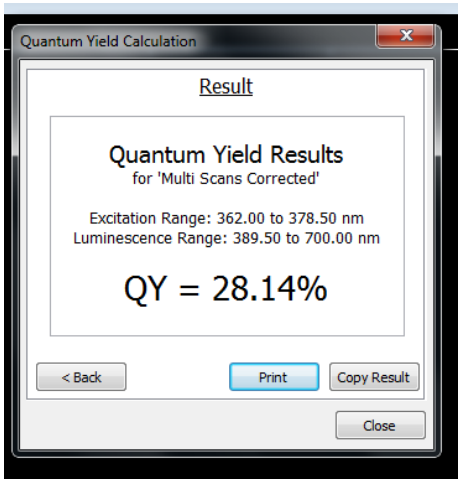

Fig. S41. The screenshot of the luminescence quantum yield of Binbox in CH_3OH measured with integration sphere.

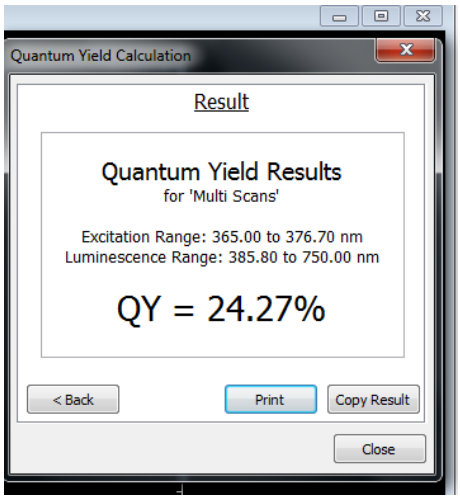

Fig. S42. The screenshot of the luminescence quantum yield of G1@Binbox in CH_3OH measured with integration sphere.

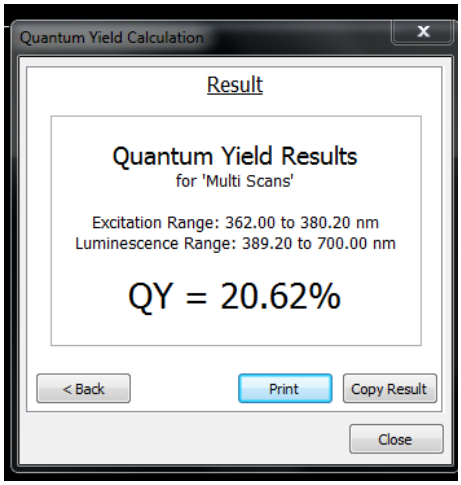

Fig. S43. The screenshot of the luminescence quantum yield of G2@Binbox in CH_3OH measured with integration

sphere.

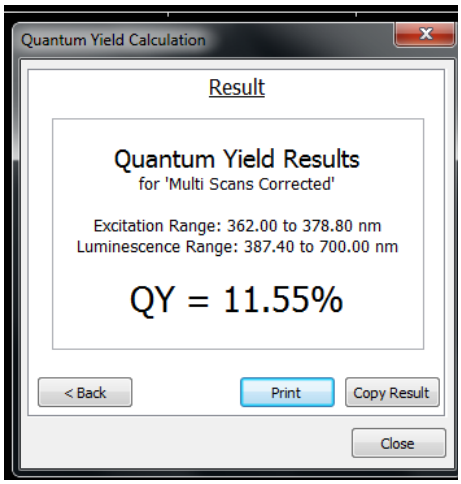

Fig. S44. The screenshot of the luminescence quantum yield of G3@Binbox in CH_3OH measured with integration sphere.

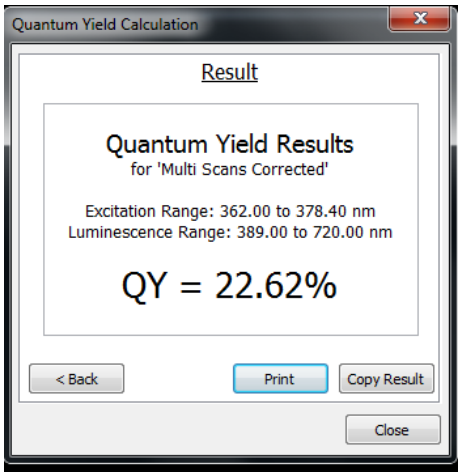

Fig. S45. The screenshot of the luminescence quantum yield of G4@Binbox in CH_3OH measured with integration sphere.

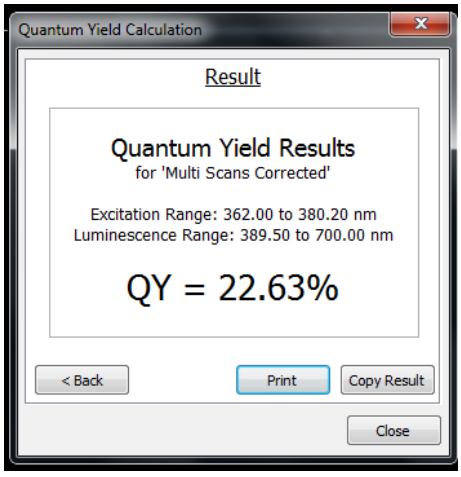

Fig. S46. The screenshot of the luminescence quantum yield of G5@Binbox in CH_3OH measured with integration sphere.

2.5 PL and CPL spectra of host-guest combination

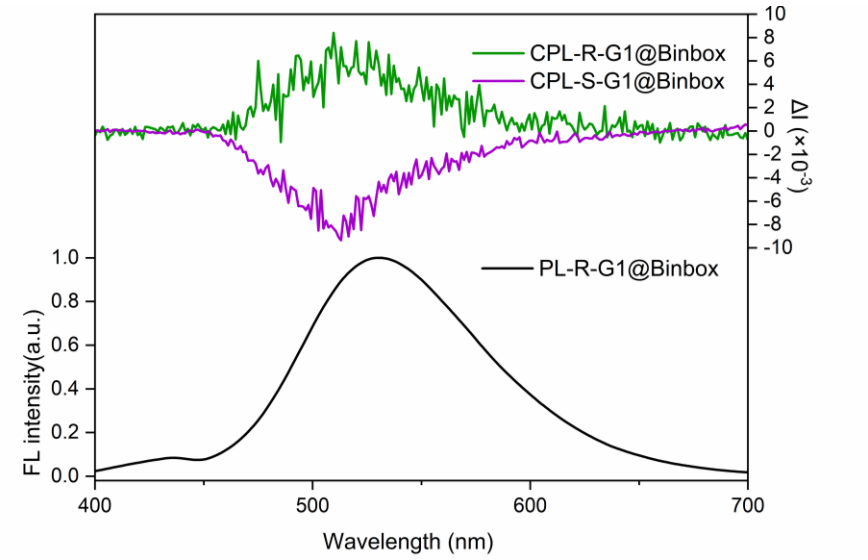

Fig. S47. PL and CPL spectra of the G1@Binbox (c = 1.0 × 10^{-5} M).

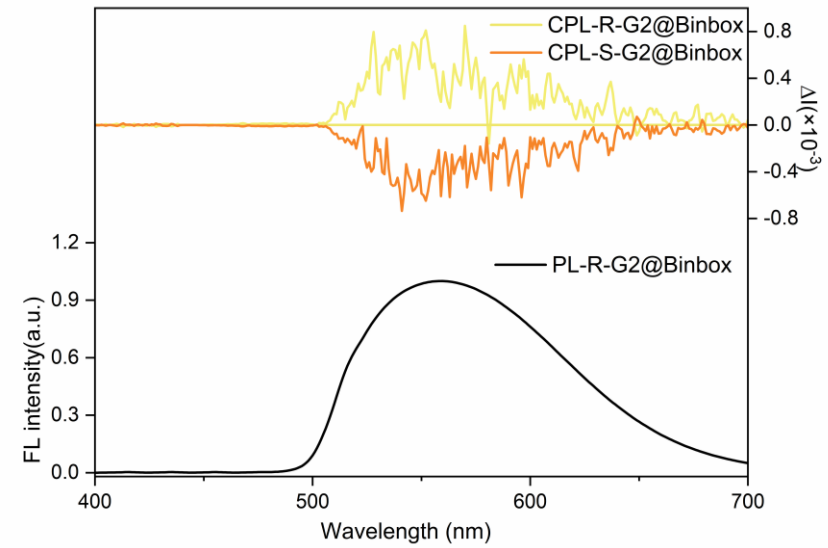

Fig. S48. PL and CPL spectra of the G2@Binbox (c = 1.0 × 10^{-5} M).

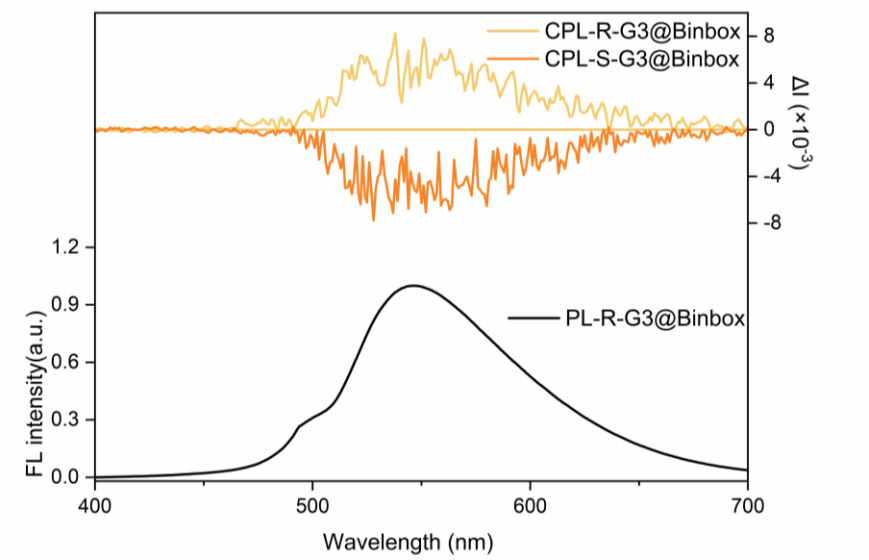

Fig. S49. PL and CPL spectra of the G3@Binbox (c = 1.0 × 10^{-5} M).

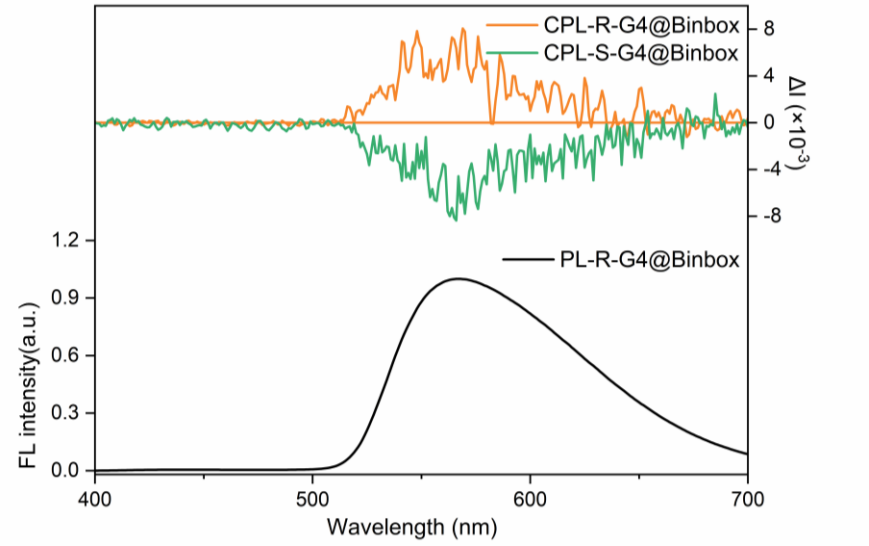

Fig. S50. PL and CPL spectra of the G4@Binbox (c = 1.0 × 10^{-5} M).

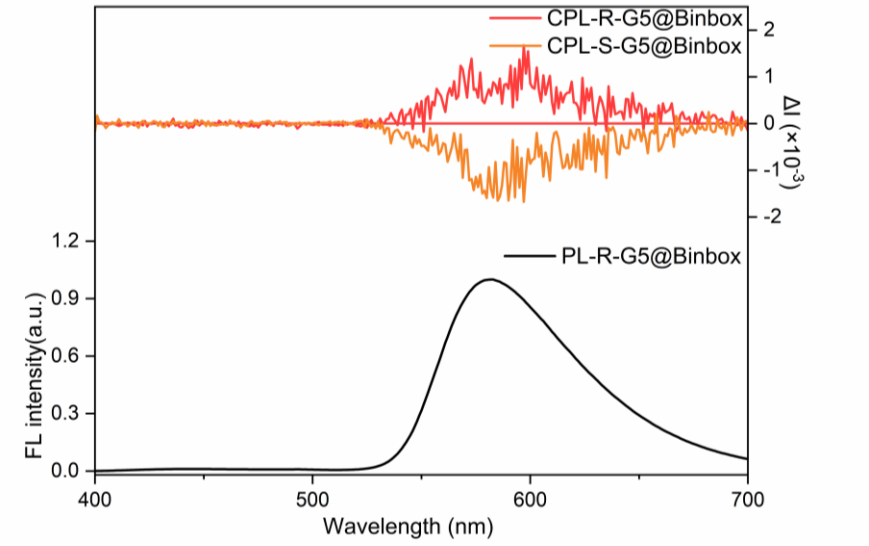

Fig. S51. PL and CPL spectra of the G5@Binbox (c = 1.0 × 10^{-5} M).

3. Host-guest complexation studies

^{1}H NMR titrations were conducted on a Bruker Avance III 400 MHz spectrometer and the chemical shifts are referenced internally to tetramethylsilane (TMS) or solvents in parts per million (ppm). In all cases, ^{1}H NMR titrations were performed maintaining the concentration (usually around 1.0×10^{-2} M) of the host constant in CD_3CN or CD_3OD.

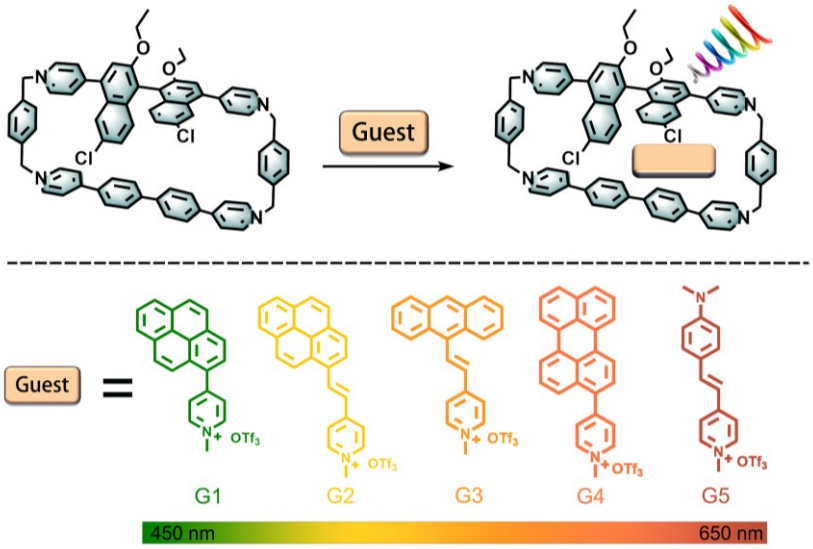

Figure S52. Binding constants of Binbox to accommodate various guests in either CD_3CN or CD_3OD. Determined by ^{1}H NMR titration.

Dissolve an achiral guest (100 equivalents, achiral planar fluorescent molecules) in CD_3CN or CD_3OD inside an NMR tube. Add varying equivalents of the achiral planar fluorescent molecules to the achiral CD_3CN or CD_3OD solution.Use a 10 μL pipette for precise addition into the Binbox. Monitoring the chemical changes within the Binbox allows straightforward tracking of host-guest complex formation.The dates were analysed with the Bindfit web-based app at Supramolecular.org - Binding Constant Calculators Supramolecular.

Table 1. Binding constants (Ka), fluorescence lifetimes (τ), Quantum efficiency (Yield), and induced g_{lum} values of Binbox and G1-G5@Binbox.

Host/Guest	K_a (10^2)	τ_1 (ns)	τ_2 (ns)	Yield (%)	g_{lum} (10^{-3})
Binbox		1.49	1.49	28.14	4.00
Binbox@G1	7.35	1.11	5.05	24.27	3.00
Binbox@G2	8.45	1.12	2.59	20.62	1.20
Binbox@G3	9.70	1.07	4.01	11.15	4.30
Binbox@G4	6.46	1.11	3.59	22.63	3.50
Binbox@G5	6.66	1.29	4.21	22.62	2.50

3.1 G1@Binbox properties and exchange constants determination

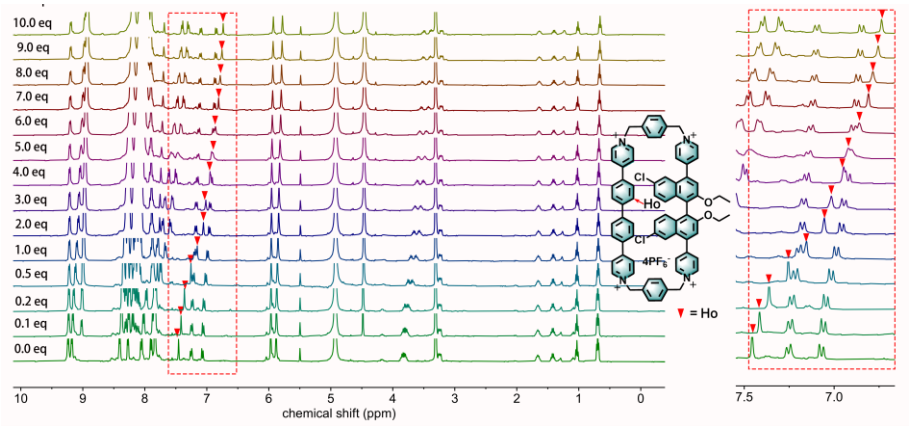

Figure S53. ^{1}H NMR spectra of titration of G1@Binbox in CD_3OD.

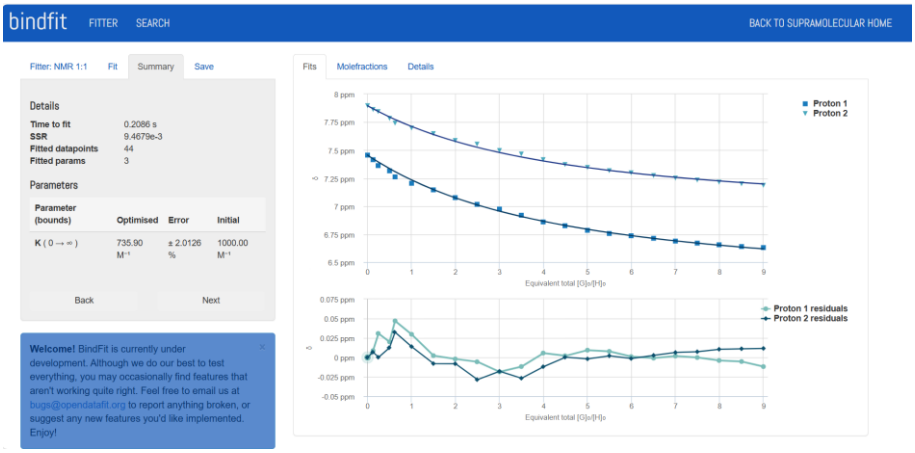

Figure S54. Screenshot from the result window of supramolecular.org which was fitted to 1:1 ^{1}H NMR binding data. This screenshot shows the raw vs. fitted data (top) and the corresponding residual plot.

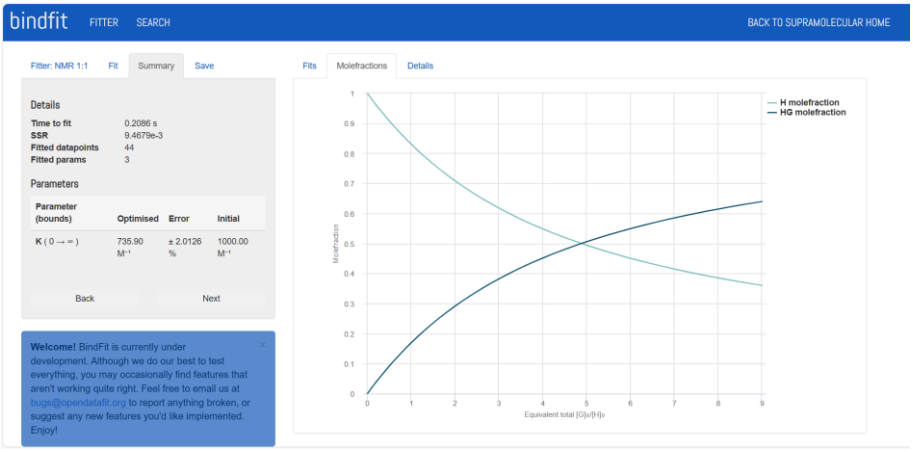

Figure S55. Screenshot from the result window of supramolecular.org which was fitted to 1:1 ^{1}H NMR binding data. This screenshot shows the calculated molefractions.

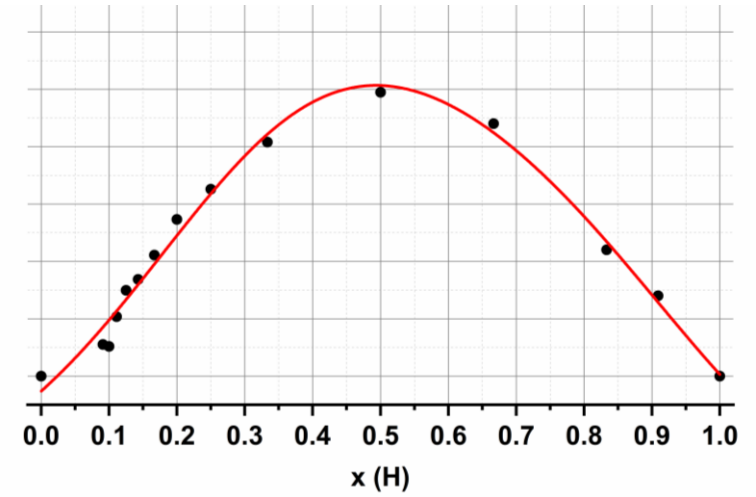

Figure S56. The job plots and residuals of G1@Binbox in CD_3OD.

3.2 G2@Binbox properties and exchange constants determination

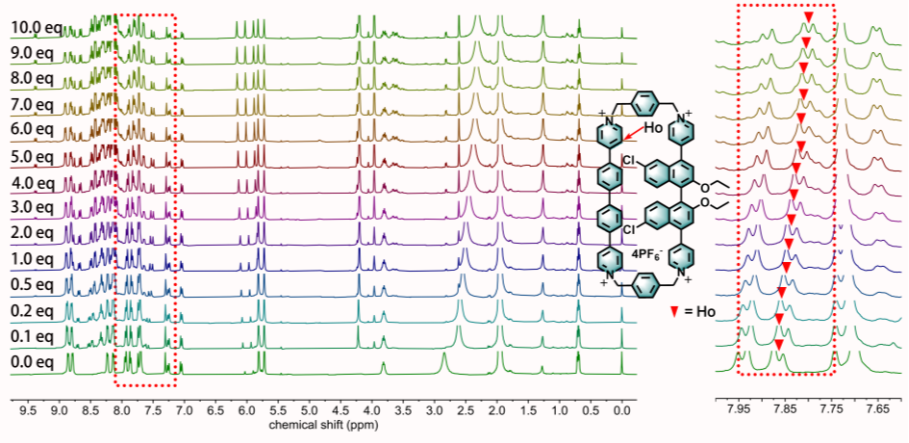

Figure S57. ^{1}H NMR spectra of titration of G2@Binbox in CD_3OD.

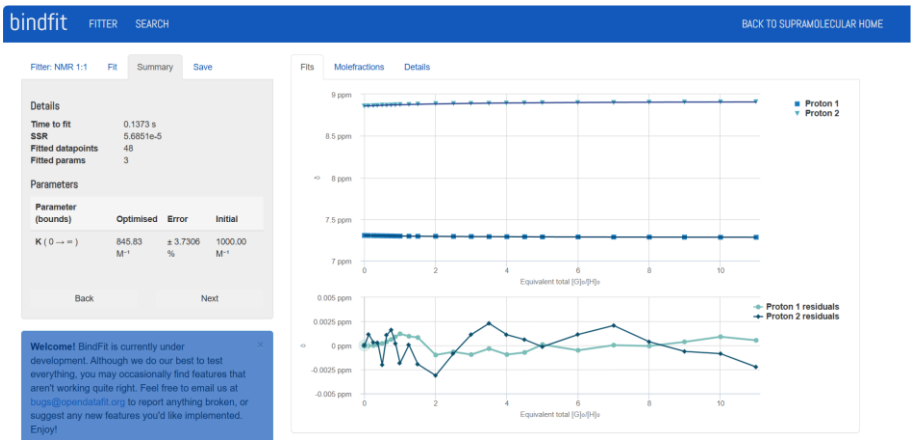

Figure S58. Screenshot from the result window of supramolecular.org which was fitted to 1:1 ^{1}HNMR binding data. This screenshot shows the raw vs. fitted data (top) and the corresponding residual plot.

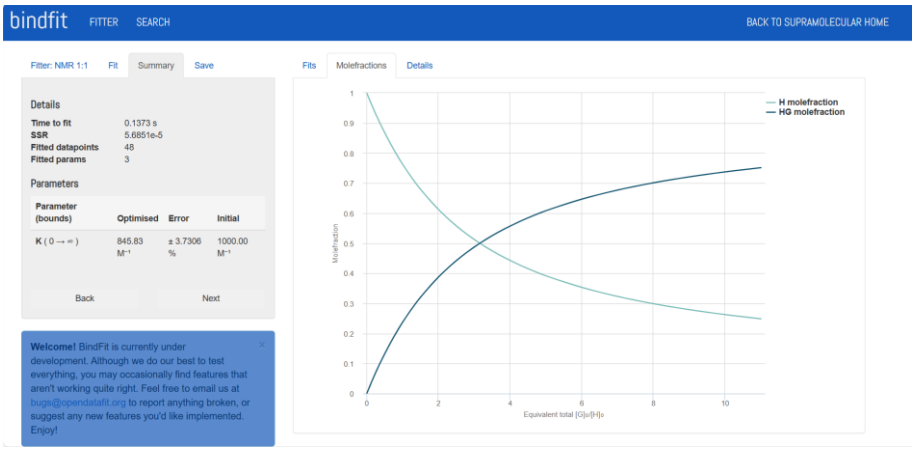

Figure S59. Screenshot from the result window of supramolecular.org which was fitted to 1:1 ^{1}H NMR binding data. This screenshot shows the calculated molefractions.

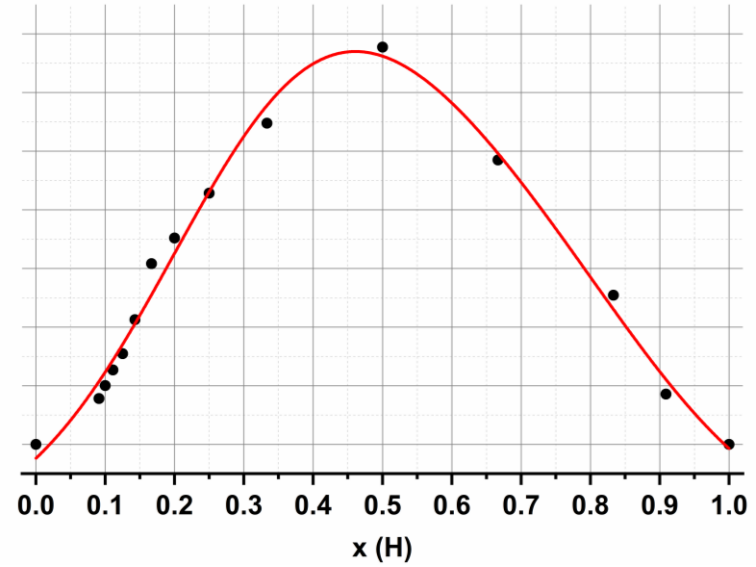

Figure S53. The job plots and residuals of G2@Binbox in CD_3OD.

3.5 G3@Binbox properties and exchange constants determination

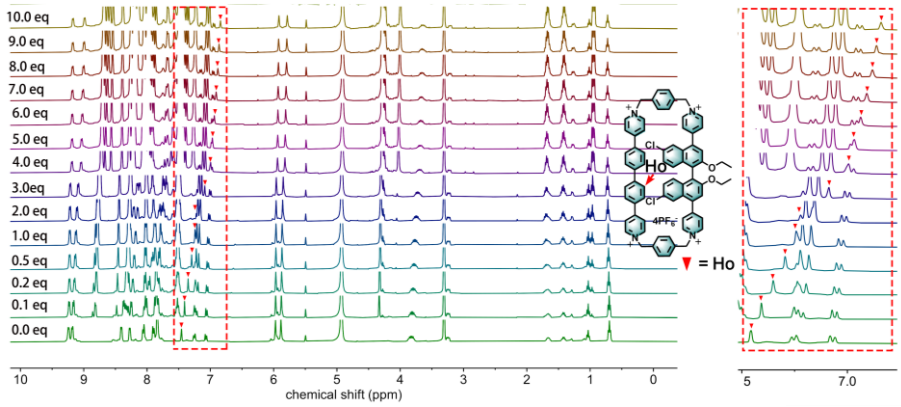

Figure S60. ^{1}H NMR spectra of titration of G3@Binbox in CD_3OD.

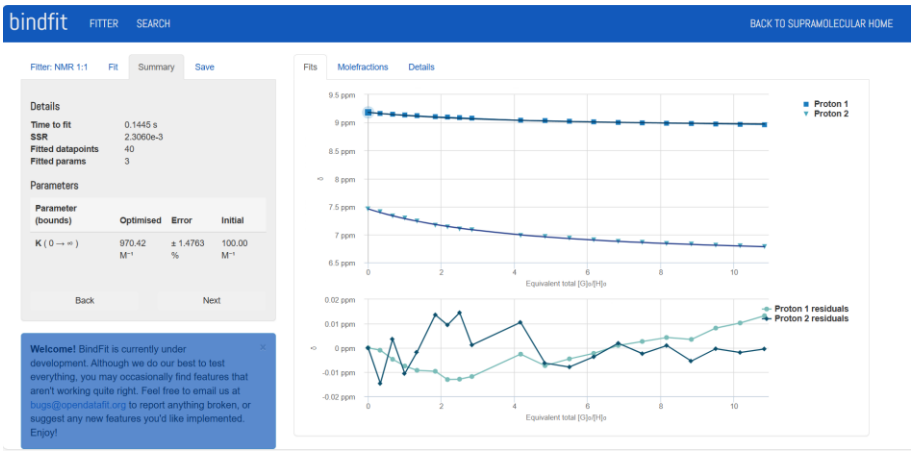

Figure S61. Screenshot from the result window of supramolecular.org which was fitted to 1:1 ^{1}H NMR binding data. This screenshot shows the raw vs. fitted data (top) and the corresponding residual plot.

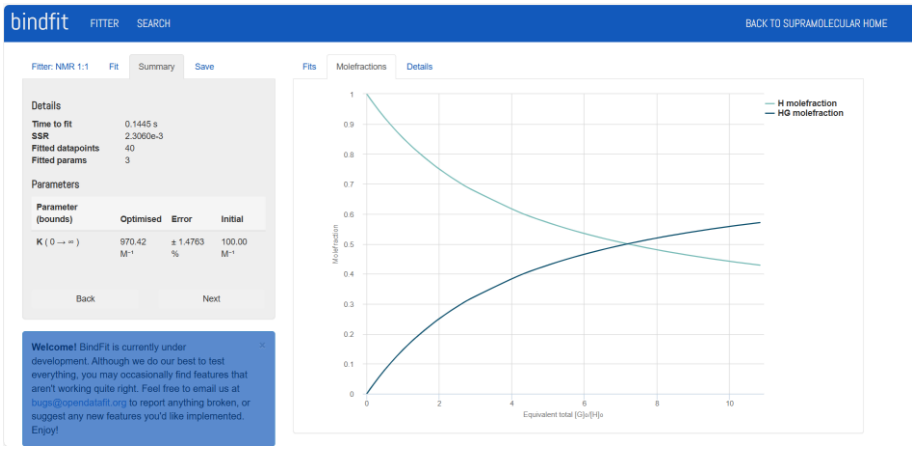

Figure S62. Screenshot from the result window of supramolecular.org which was fitted to 1:1 ^{1}H NMR binding data. This screenshot shows the calculated molefractions.

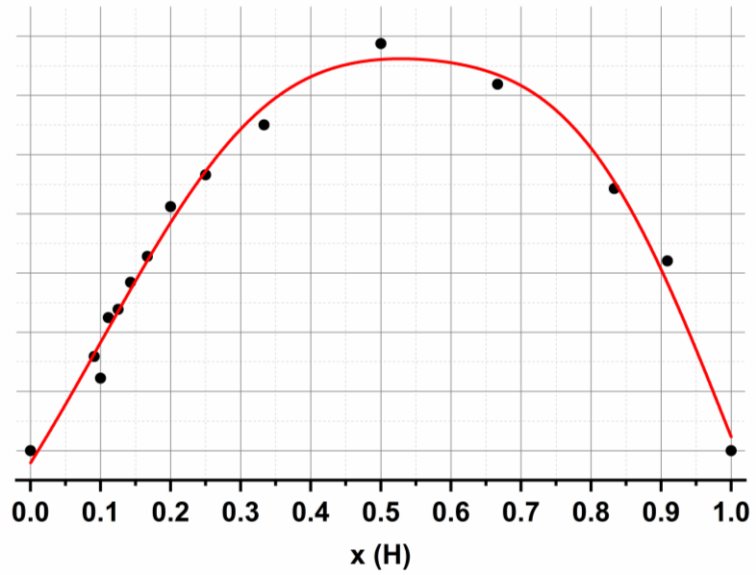

Figure S63. The job plots and residuals of G3@Binbox in CD_3OD.

3.4 G4@Binbox properties and exchange constants determination

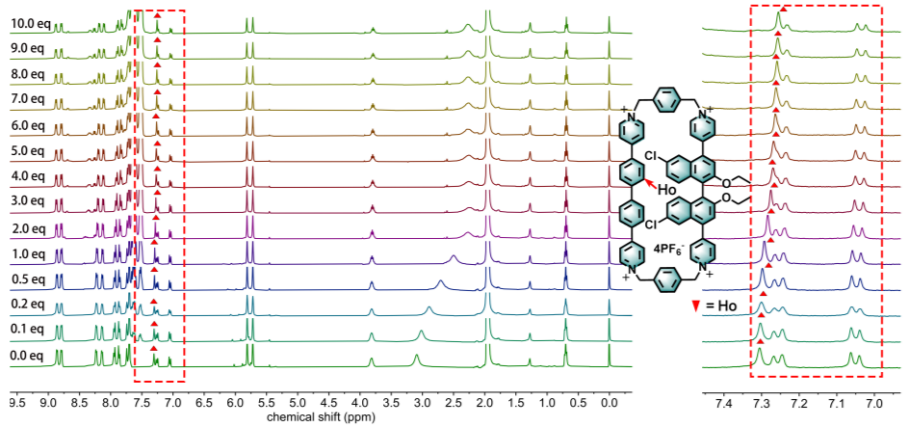

Figure S64. ^{1}H NMR spectra of titration of G4@Binbox in CD_3OD.

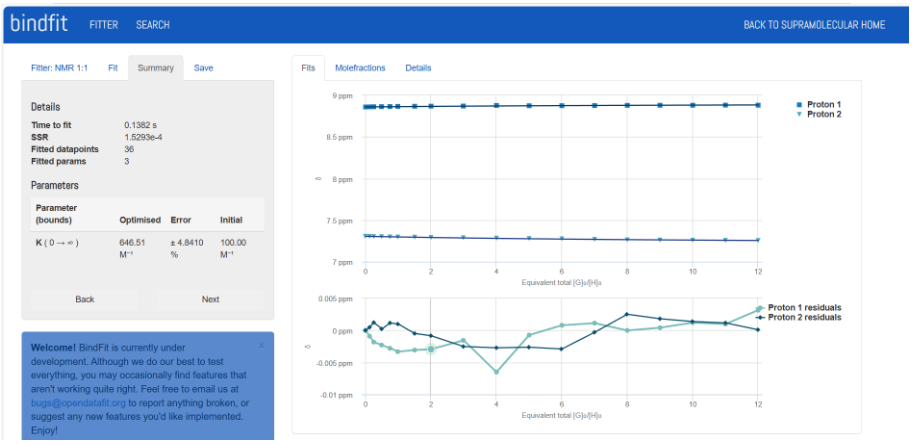

Figure S65. Screenshot from the result window of supramolecular.org which was fitted to 1:1 ^{1}H NMR binding data. This screenshot shows the raw vs. fitted data (top) and the corresponding residual plot.

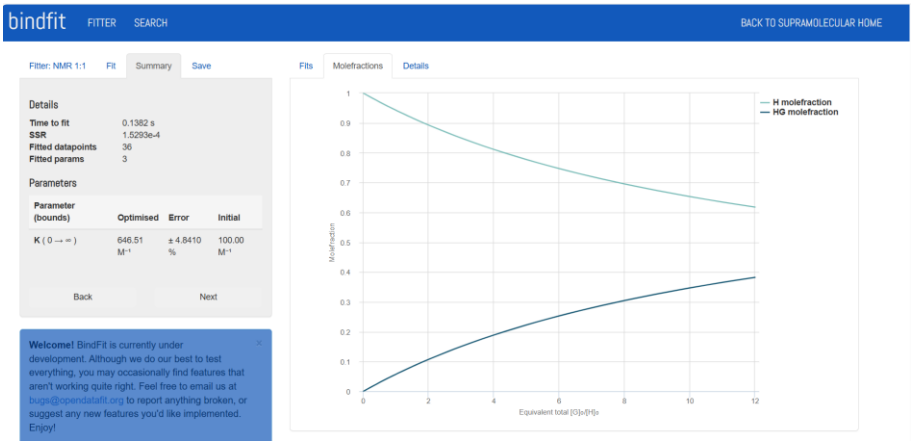

Figure S66. Screenshot from the result window of supramolecular.org which was fitted to 1:1 ^{1}H NMR binding data. This screenshot shows the calculated molefractions.

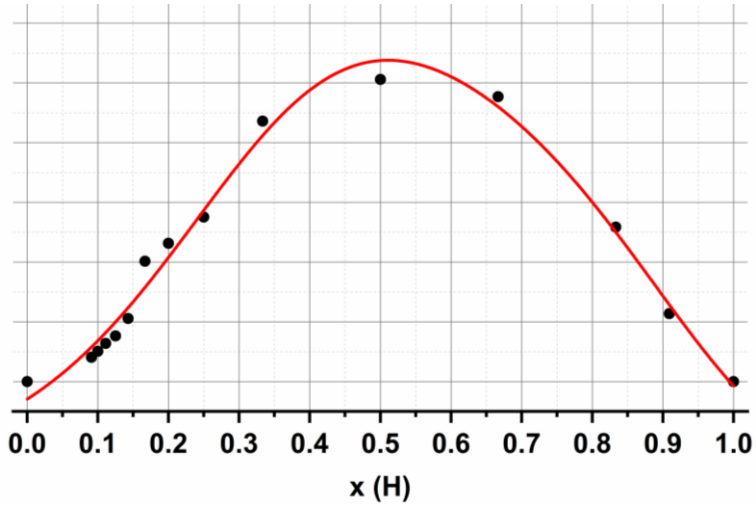

Figure S67. The job plots and residuals of G4@Binbox in CD_3OD.

3.3 G5@Binbox properties and exchange constants determination

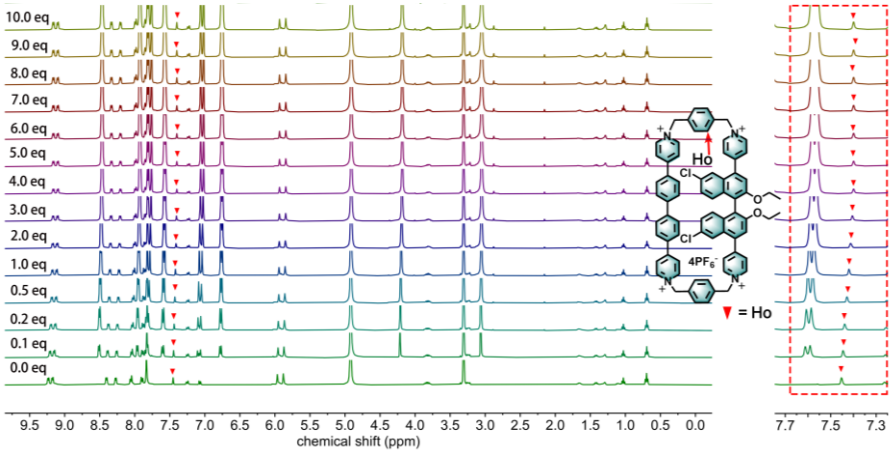

Figure S68. ^1H NMR spectra of titration of G5@Binbox in CD_3OD.

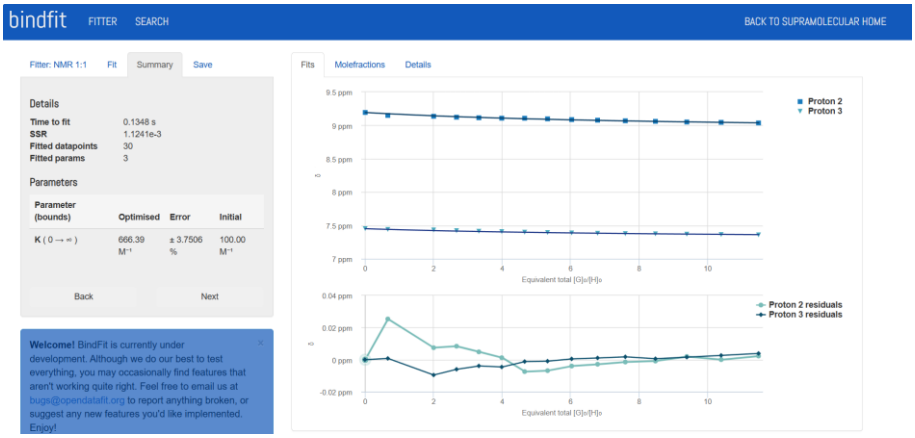

Figure S69. Screenshot from the result window of supramolecular.org which was fitted to 1:1 ^1H NMR binding data. This screenshot shows the raw vs. fitted data (top) and the corresponding residual plot.

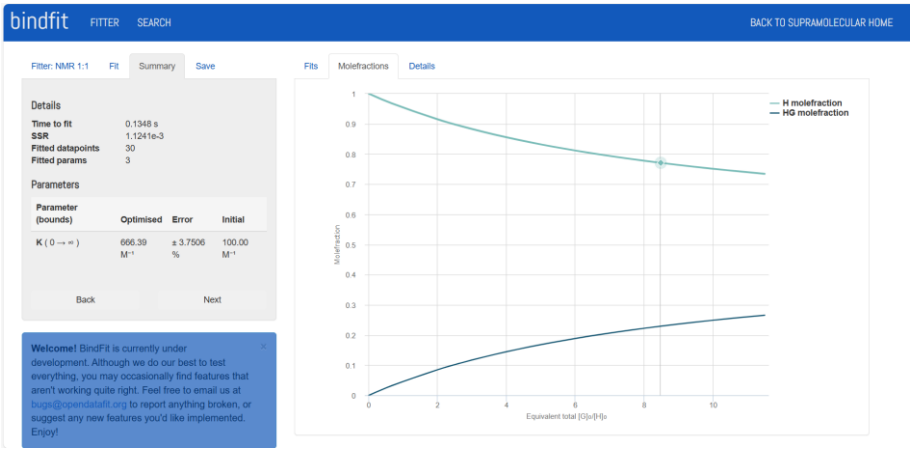

Figure S70. Screenshot from the result window of supramolecular.org which was fitted to 1:1 ^{1}H NMR binding data. This screenshot shows the calculated molefractions.

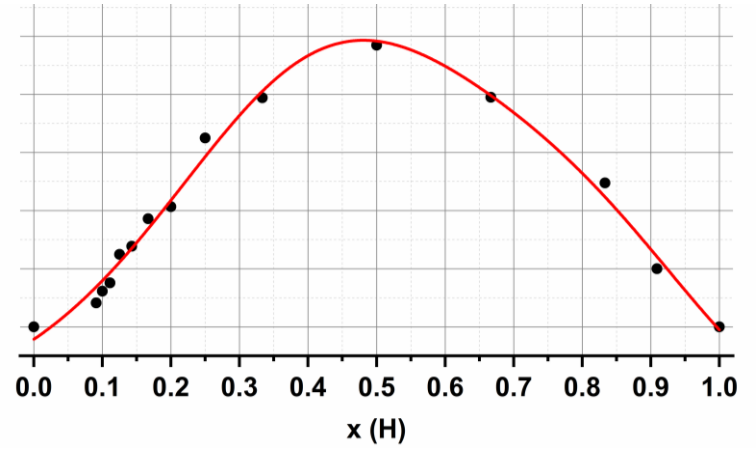

Figure S71. The job plots and residuals of G5@Binbox in CD_3OD.

4. DFT and Hirshfeld

4.1 Calculation Details

All DFT calculations were performed using the Gaussian16 C.01 software package.[1] Geometry optimizations were carried out using DFT calculations with the b3lyp-D3 functional.[2] The 6-31G* basis set was used for all atoms.[3-4] TD-DFT excited-state calculations of host-guest complexes were also performed using the Gaussian16 C.01 software package. During the calculations, the b3lyp/6-311G* basis set was used.[5] The first 5 monoelectronic excitations were calculated and the transition dipole moment of ligand was visualized using Multiwfn and VMD.[6–7]

The Geometry center and Fragment transition dipole moment are listed below.

Electric dipole transition coordinate

Geometry center: 4.889585018157959 -0.7927072644233704 2.456634283065796

Fragment transition dipole moment: -0.15991099999999997 0.027513000000000003 -0.075571

Magnetic dipole transition coordinate

Geometry center: 4.889585018157959 -0.7927072644233704 2.456634283065796

Fragment transition dipole moment: 0.006125 -0.053389000000000006 -0.10585900000000001

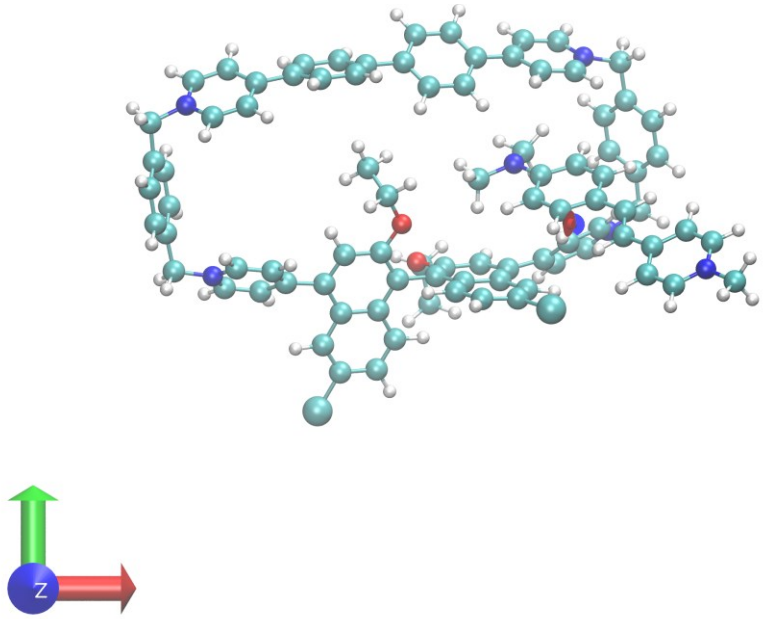

Figure S72. Magnetic dipole moments and electric dipole moment vectors of dye fragments in the host-guest system

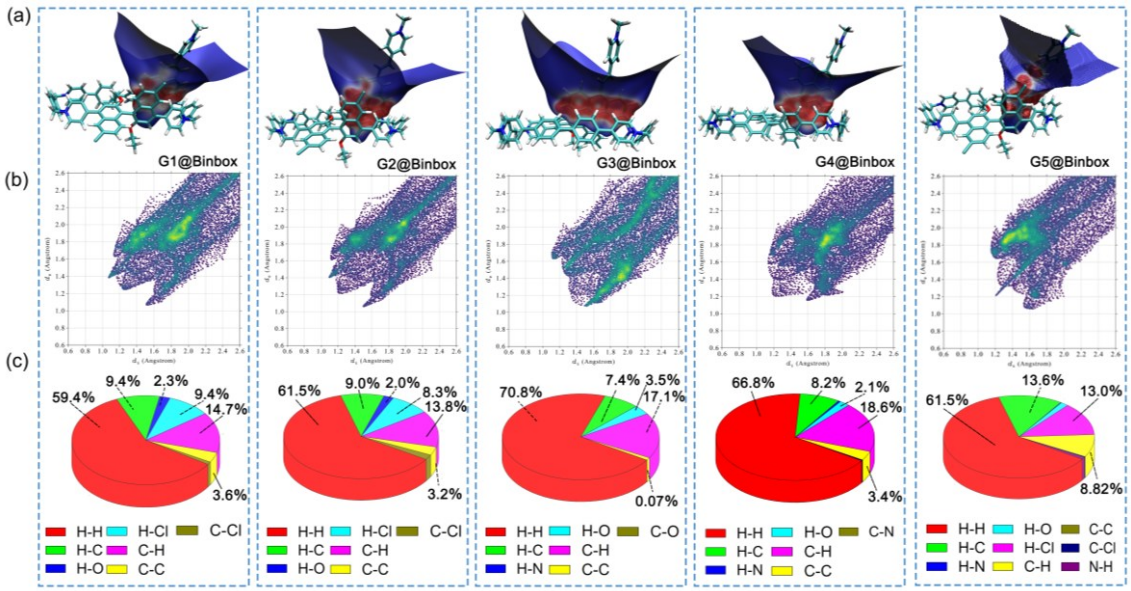

Figure S73. (a) Hirshfeld surfaces of G1-G5@Binbox (b) 2D fingerprint plots for G1-G5@Binbox. (c) Percentage contributions of the average interactions for G1-G5@Binbox.

5. Crystallographic Characterization

All crystallographic data are available free of charge from the Cambridge Crystallographic Data Centre (CCDC) via www.ccdc.cam.ac.uk/data_request/cif. CCDC number 2539057.

Method. BinBox (3.4 mg, 2.4 µmol) was dissolved in MeCN (0.8 mL) and the mixture was passed through a 0.45 µm filter equally into three 1 mL tubes. The tubes were placed together in one 20 mL vial containing iPr_2O (~3 mL) and the vial was capped. Slow vapor diffusion of iPr_2O into the solution of BinBox in MeCN (3.0 mM) over the course of one week yielded colorless single crystals of BinBox. Data were collected at 100 K on a Bruker Kappa $APEX_2$ CCD Diffractometer equipped with a MoKα microsource with Quazar optics. The solid-state structure of BinBox is shown in Figure S1.

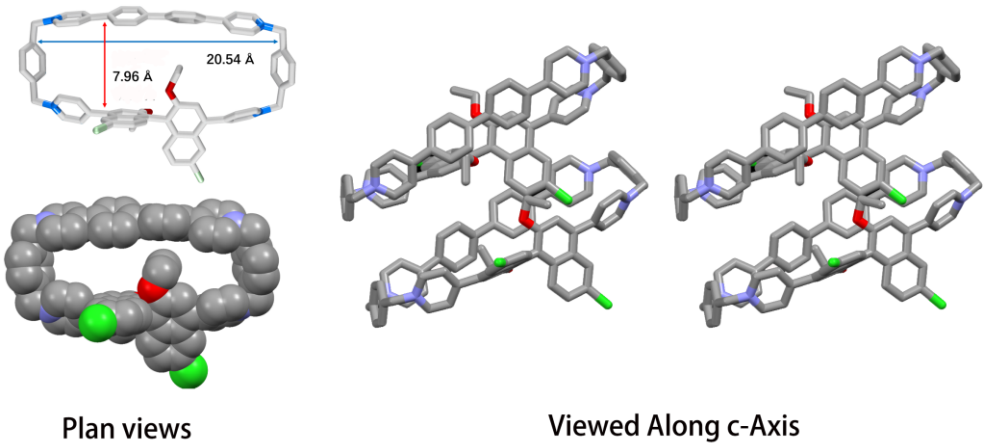

Figure S74. Different crystallographic views of BinBox. Counterions and solvent molecules are omitted for the sake of clarity.

Table 2. Crystal data of Binbox.

	Binbox
CCDC number	2539057
Empirical formula	$C_{74}H_{61}Cl_2F_{24}N_5O_2P_4$
Formula weight	1703.05
Temperature/K	193.0
Crystal system	monoclinic
Space group	$P2_1\ 2_1\ 2_1$
a/Å	25.018(3)
b/Å	14.1085(15)
c/Å	43.383(5)
α(deg)	90
β(deg)	90.069(4)
γ(deg)	90
Volume/Å^3	15313(3)
Z	8
ρ_{calc}g/cm^3	1.477
μ/mm^{-1}	0.276
F(000)	6928.0
R1	0.1984,
wR_2	0.3653
R_1	0.2687
wR_2	0.3994
Goodness-of-fit on F^2	1.134

2. References

[1] DFT calculations were performed using Gaussian16, revisionC.01; M. J. Frisch, G. W. Trucks, H. B. Schlegel, G. E. Scuseria, M. A. Robb, J. R. Cheeseman, G. Scalmani, V. Barone, G. A. Petersson, H. Nakatsuji, X. Li, M. Caricato, A. V. Marenich, J. Bloino, B. G. Janesko, R. Gomperts, B. Mennucci, H. P. Hratchian, J. V. Ortiz, A. F. Izmaylov, J. L. Sonnenberg,D. Williams-Young, F. Ding, F. Lipparini, F. Egidi, J. Goings, B. Peng, A. Petrone, T. Henderson, D. Ranasinghe, V. G. Zakrzewski, J. Gao, N. Rega, G. Zheng, W. Liang, M. Hada, M. Ehara, K. Toyota, R. Fukuda, J. Hasegawa, M. Ishida, T. Nakajima, Y. Honda, O. Kitao, H. Nakai, T. Vreven, K. Throssell, J. A. Montgomery, Jr., J. E. Peralta, F. Ogliaro, M. J. Bearpark, J. J. Heyd, E. N. Brothers, K. N. Kudin, V. N. Staroverov, T. A. Keith, R. Kobayashi, J. Normand, K. Raghavachari, A. P. Rendell, J. C. Burant, S. S. Iyengar, J. Tomasi, M. Cossi, J. M. Millam, M. Klene, C. Adamo, R. Cammi, J. W. Ochterski, R. L. Martin, K. Morokuma, O. Farkas, J. B. Foresman and D. J. Fox, Gaussian, Inc.: Wallingford CT, 2016.

[2] Grimme, S.; Ehrlich, S.; Goerigk, L. Effect of the damping function in dispersion corrected density functional theory. *J. Comput. Chem.***2011**, 32, 1456–1465.

[3] M. Dolg, U. Wedig, H. Stoll and H. Preuss, Energyadjusted ab initio pseudopotentials for the first row transition elements, *J. Chem. Phys.*, 1987, **86**, 866−872.

[4] J. M. L. Martin and A. Sundermann, Correlation consistent valence basis sets for use with the Stuttgart-Dresden-Bonn relativistic effective core potentials: The atoms Ga–Kr and In–Xe, *J. Chem. Phys.*, 2001, **114**, 3408−3420.

[5] R. Bauernschmitt and R. Ahlrichs, Treatment of electronic excitations within the adiabatic approximation of time dependent density functional theory. *Chem. Phys. Lett.*, 256, 454–464.

[6] T. Lu, F. Chen, Multiwfn: a multifunctional wavefunction analyzer, *J. Comput. Chem.*, 2012, **33**, 580−592.

[7] W. Humphrey, A. Dalke and K. Schulten, VMD: visual molecular dynamics, *J. Mol. Graphics.*, 1996, **14**, 33−38

Bauernschmitt, R., & Ahlrichs, R. (1996). Treatment of electronic excitations within the adiabatic approximation of time dependent density functional theory. *Chemical Physics Letters*, 256, 454–464.